A UQ based calibration for the CFD modeling of the gas dispersion from an LNG pool

Marco Bellegoni[a], Claudio Chicchiero[a,*], Gabriele Landucci[a], Chiara Galletti[a], Maria Vittoria Salvetti[a]

[a] *Department of Civil and Industrial Engineering, University of Pisa, Italy*

Abstract

The modeling with Computational Fluid Dynamics (CFD) of gas dispersion from a liquified natural gas (LNG) pool is investigated in detail to better elucidate the sources of uncertainties and the influence of physical phenomena, such as convection and diffusion, just above the pool. Indeed, a better comprehension of these topics can improve gas dispersion analysis and aid the implementation of mitigation measures. However, the literature shows a lack of knowledge on this matter, since the LNG pool inlet conditions have not been precisely analyzed so far. To this purpose, the present work proposes, for the first time in this field, the application of an Uncertainty Quantification (UQ) technique to calibrate the inlet conditions of a CFD model for cloud dispersion from a LNG pool. More specifically, the Burro test series is used to validate numerical simulations based on the solution of Unsteady Reynolds-averaged Navier-Stokes (URANS) equations. As the LNG is released into a water pool, the real LNG pool radius is unknown. Moreover, the gas release is also unknown as it is not equal to the LNG spill rate. ~~A preliminary evaluation of the average LNG pool radius is done by employing an integral model. Then, CFD simulations are carried out with this radius by considering a purely convective, a purely diffusive and a convective-diffusive inlet flow. Both the first two approaches lead to uncertainties or unphysical results; hence, a calibration is performed with the latter model by applying an Uncertainty Quantification technique.~~ The generalized Polynomial Chaos (gPC) expansion is therefore used to estimate these uncertain parameters~~the gas pool radius and the mass flow rate~~, by minimizing the errors between CFD and available measurements. The optimization performed on the Lower Flammable Limit (LFL) concentration maps shows how this procedure can give a very good agreement with the experimental observations, extending the accuracy of CFD simulations within risk assessment studies. Besides, this approach highlights how the influence of convection and diffusion on the simulation results strongly depends on the wind conditions. In this manner, the present work can help modelers to better setup CFD simulations with the purpose to aid the decision making in the process safety framework. ~~characteristics of the Atmospheric Boundary Layer (ABL).~~

*Corresponding author: e-mail claudio.chicchiero@phd.unipi.it

Nomenclature

$C_{\epsilon 1}$	k-ϵ model constant
$C_{\epsilon 2}$	k-ϵ model constant
$C_{\epsilon 3}$	k-ϵ model constant
C_μ	k-ϵ model constant
c_p	Specific heat capacity [J/(Kg K)]
C_s	Empirical constant for roughness height
D_k	Molecular diffusivity of k-th chemical species [m^2/s]
D_t	Turbulent diffusivity [m^2/s]
g	Gravitational acceleration [m/s^2]
k	Turbulent kinetic energy [m^2/s^2]
K_s	Roughness height [m]
k_T	Thermal conductivity [W/(m K)]
L	Monin-Obukhov length [m]
$\dot{m}$	Imposed mass flow rate [kg/s]
$M_{w,k}$	Molecular weight of the $k-$th species [g/mol]
P	Pressure [Pa]
P_j	Maximum degree of gPC polynomials for the j-th parameter
p_{op}	Operating pressure [Pa]
R	Methane inlet radius [m]
$\mathcal{R}$	Universal gas constant [J/(mol K)]
Sc_t	Turbulent Schmidt number
S_ϵ	Source term for ϵ [$kg/(m\,s^4)$]
T	Temperature [K]
t	Time [s]
T_W	Wall temperature [K]
T_*	Friction temperature [K]
U_i	i-th component of velocity [m/s]
u_*	Friction velocity [m/s]
w	Weight function of quadrature integration
Y_k	Mass fraction of k-th chemical species
z	Height above ground [m]
z_0	Surface roughness [m]
z_p	Height of wall-adjacent cell-centroid [m]
β	Coefficients of gPC expansion
δ	Kronecker delta
Δt	Time step of simulation [s]
ϵ	Turbulent dissipation rate [m^2/s^3]
κ	von Kàrmàn constant
ν	Molecular kinematic viscosity [m^2/s]
ν_t	Turbulent kinematic viscosity [m^2/s]
Φ_ϵ	Semi-empirical function for atmospheric stability
Φ_m	Semi-empirical function for atmospheric stability
ψ	Basis functions of gPC expansion
ρ	Weighted density of air/methane mixture [kg/m^3]
σ_ϵ	k-ϵ model constant
σ_k	k-ϵ model constant
ζ	Support variable of gPC expansion
ASsM	Atmospheric Stability sub-Model
gPC	generalized Polynomial Chaos

LFL Lower Flammable Limit

LNG Liquified Natural Gas

LPG Liquified Petroleum Gas

PDF Probability Density Function

RPT Rapid Phase Transition

UQ Uncertainty Quantification

URANS Unsteady Reynolds-averaged Navier-Stokes (equations)

1. Introduction

The prevention of accidents both in industrial sites and in the urban context, involving hazardous materials like flammable or toxic substances is a critical task (Guo et al., 2020; Mishra, 2015; Pontiggia et al., 2011; Hanna et al., 2009). For this purpose, devising systems of environmental protection as well as improving process safety need the availability of accurate models, which should be able to predict the dispersion of pollutants or hazardous substances in the environment. Indeed, experimental data alone are not sufficient for making accurate predictions about gas dispersion (Moen et al., 2019; Tan et al., 2018).

The most frequently used models for this purpose are integral ones, based on lumped parameters. These models rely on basic equations, which describe the relevant phenomena using empirical correlations, often leading to an overprediction of the consequences. Moreover, since these empirical correlations are derived in specific conditions, i.e., mostly open-field configurations, the integral models are intrinsically unable to take into account the presence of obstacles in the domain (Busini & Rota, 2014; Pontiggia et al., 2009). This drawback poses serious limitations to their applicability, as obstacles are often present, for instance, in the form of buildings in urban areas or storage tanks or process equipment in industrial plants.

For this reason, increasing attention is paid to Computational Fluid Dynamics (CFD) as a promising tool to perform risk assessment studies as well as analysis on environmental impact (Horvat, 2018; Allegrini et al., 2014; Cant et al., 2004). CFD solves the 3-dimensional equations of fluid dynamics, i.e., Navier-Stokes equations, coupled with the transport equation of chemical species in complex layouts and scenarios. One of the main drawbacks is the high computational cost since this kind of problem can concern large domains with complex geometries, where numerous equations have to be solved in a huge number of small spatial volumes and at several time instants used for discretization. Hence, simplified models are usually adopted for some of the relevant physical phenomena as for instance by applying a Reynolds-averaging of the governing equations to treat turbulence.

Several works have been performed using CFD to analyze gas dispersion in different scenarios within process safety and risk management studies. For instance, CFD has been employed for simulating gas dispersion in the urban context by both validation studies (Guo et al., 2020; Tan et al., 2018; Habib et al., 2014; Tauseef et al., 2011) and analysis on real or possible accidental releases (Pontiggia et al., 2011, 2010a). Besides, also industrial layouts have been considered in the use of CFD simulations, especially for cryogenics releases (Schleder & Martins, 2016; Liu et al., 2016; Fiates et al., 2016; Labovský

& Jelemenský, 2010). Finally, CFD has been demonstrated as a valuable source for the support in the development of mitigation measures like gas detectors networks (Cen et al., 2018; Rad et al., 2017; Vázquez-Román et al., 2016). For instance, CFD has been compared against conventional tools adopted in the framework of gas dispersion studies by (Habib et al., 2014), showing its good accuracy with different boundary conditions and experimental setups. Moreover, Tan et al. (2018) carried out CFD simulations of heavy gas dispersion validating them against experimental measurements on a wind tunnel test case replicating an urban street canyon. In a similar way, Tauseef et al. (2011) performed an analysis of dense gas release with a precise characterization of the flow field near a simple obstacle, being able to accurately predict the vortices and recirculation zones.

Remaining in the urban framework, Guo et al. (2020) validated a CFD model with the well-known experimental test MUST (Biltoft, 2001). This study allowed to analyze the effect of different classes of atmospheric stability on gas dispersion. Besides, Pontiggia et al. (2010a) used CFD modeling to assess the consequences of ammonia dispersion in a real urban case study, proving its reliability in this context. Another notable CFD assessment of gas dispersion in urban areas has been performed in (Pontiggia et al., 2011) with simulations of the Viareggio accidental scenario of Liquified Petroleum Gas (LPG) release.

The use of CFD models has also been considered within industrial framework and cryogenics gas dispersion. For example, Schleder & Martins (2016) and Liu et al. (2016) carried out simulation on the dispersion from CO_2 releases, while Fiates et al. (2016) performed also a characterization of the carbon dioxide emission source, making a comparison with Liquified Natural Gas (LNG) releases. Labovský & Jelemenský (2010) investigated the accuracy of CFD with an ammonia dispersion study, validated against FLADIS experimental case (Nielsen et al., 1997).

Furthermore, CFD has been applied also to the development of risk reduction systems like gas detectors in industrial storage plants. As a matter of fact, a lot of studies have been dedicated to the use of CFD simulations data to build algorithms for the optimal placement of gas sensors (Cen et al., 2018; Rad et al., 2017; Vázquez-Román et al., 2016).

From the above literature review it can be noticed how CFD models can be used as a promising tool to assess the consequences of accidental scenarios and to support the risk analysis studies in the framework of chemical and process industries. However, CFD models for gas dispersion analysis are affected by sources of uncertainties (Gerbec et al., 2017; Tominaga & Stathopoulos, 2013), that have not been considered in the process safety framework. These uncertainties may potentially affect the reliability of impact predictions as well as the potential implementation in risk studies.

Indeed, the models used to take into account turbulence introduce sources of uncertainties (Gerbec et al., 2017; Tominaga & Stathopoulos, 2013) that should be carefully analyzed. It is of primary importance to investigate these sources of uncertainties with the aim of building accurate and reliable models for the prediction of gas dispersion and, consequently, support the design of mitigation and risk reduction measures.

In the context of gas dispersion analysis, the CFD model should first ensure accurate wind profiles

~~throughout all the computational domain in an open field configuration, thus providing a good description of the Atmospheric Boundary Layer (ABL)~~ (Blocken et al., 2007; Jörg Franke, Antti Hellsten, Heinke Schlünzen, 2007; Tominaga & Stathopoulos, 2007). ~~Indeed the ABL plays a major role in gas dispersion analysis since atmospheric turbulence strongly affects the spread of a gas cloud. To this purpose, different models have been proposed in the literature for setting proper inlet conditions as well for adapting the turbulence closure equations to the ABL~~ (Parente et al., 2011; Gorlé et al., 2009; Pontiggia et al., 2009).

One recurrent problem that asks for numerical models to improve safety is the dispersion of natural gas. This energy source is playing an increasingly important role within the energy transition, especially in the form of Liquified Natural Gas (LNG) (Aneziris et al., 2020; Osorio-Tejada et al., 2017). However, the increase of LNG terminals needs safety measures to deal with the flammability of natural gas (Mishra & Mishra, 2021; Iannaccone et al., 2019). Several works have been devoted to the description of accidental releases of this material and an important aspect is represented by its vaporization behavior (Bariha et al., 2016), also in terms of consequences like flash fires (Carboni et al., 2022). As a matter of fact, LNG vaporizes as a heavy gas at first place and then vapour becomes light, enabling a better dispersion. This is different from other cryogenics like CO_2, which often reaches the triple point and presents a more complex release process (Fiates et al., 2016; Mocellin & Maschio, 2016) or Liquified Petroleum Gas (LPG), which behaves like a heavy gas throughout the whole process, being similar to pure propane (Conrado & Vesovic, 2000). ~~its demand as an energy source is growing, leading to the increase of LNG terminals that need safety measures to deal with the flammability of natural gas~~ (Mishra & Mishra, 2021; Iannaccone et al., 2019). In this scenario, the development of CFD models may benefit from some well-known experimental tests, such as Burro, Coyote and Falcon tests (Koopman et al., 1982; Goldwire et al.; Brown et al., 1990), which were carried out to better understand the LNG spill and subsequent dispersion of the gas cloud. In the Burro and Coyote test series, which involved 9 and 10 tests respectively, the LNG was spilled on a water pool ~~having a diameter of 58 m~~; subsequently, the LNG vaporized promoting the formation of a gas cloud, which was characterized by means of visualization as well of some concentration measurements. ~~These tests may provide important validation data for the general benchmark of LNG dispersion modeling with particular reference to the development of CFD tools. However, these experimental data were acquired many years ago and besides, some data showed intrinsic errors as they were obtained through interpolation of the measurements. Moreover, Rapid Phase Transition (RPT) explosions happened during some tests, causing the direct gas cloud measurement to be impossible in a large area.~~

~~Some sources of uncertainty can be identified when simulating these tests with CFD models.~~ The simulation of these tests with CFD models is affected by some sources of uncertainty which, however, have not been considered so far in the literature. ~~The common approach is to employ a single-phase model, i.e. only the gas release and dispersion are modeled. Hence the LNG pool is treated as a zone from which gaseous methane enters the computational domain.~~ One of the most relevant sources of uncertainty is the kind of inlet conditions, which must be given on the region corresponding to the LNG pool,

and determine the quantity of natural gas that enters the computational domain. ~~this depends on the different roles played by convection and diffusion. Indeed, the influence of the first phenomenon is that methane mass depends only on the gas velocity at the inlet while with diffusion, this dependence is also on the concentration gradients above the LNG pool.~~ In particular, the two main phenomena responsible for the immission of LNG into the surrounding atmosphere are convection and diffusion; their relative importance depends on the test and wind conditions. However, it is not common, in the literature, to indicate if only convection or both phenomena are considered.

As a matter of fact, several works dealing with the simulation of the above-mentioned tests can be found, for which we assume that only convection is implemented in the CFD model as no indication is present (Wu et al., 2021; Sun et al., 2013; Luketa-Hanlin et al., 2007). All these works performed URANS simulations by considering only the gas phase and treating the LNG pool as a gas velocity inlet. The inlet velocity was estimated from the experimentally measured LNG mass flux or spill rate and different numerical codes and turbulence models were used. All these works reported some discrepancies with respect to reference experimental data. ~~For instance,~~ Luketa-Hanlin et al. (2007) ~~carried out numerical simulations of the Burro 9 test. The authors solved Unsteady Reynolds-averaged Navier-Stokes (URANS) using the CFD finite-element code FEM3. The LNG pool was treated as a gas velocity inlet by computing the velocity from the LNG experimental mass flux value and imposing a turbulent intensity which, however, is not known a priori. The results reported in the paper indicated a temporal delay with respect to experimental data. More specifically, the cloud footprint predicted after $t = 120$ s matches the experimental one at $t = 80$ s.~~ Sun et al. (2013) ~~performed URANS simulations of gas dispersion in the Burro 5 and 8 tests. The inlet gas velocity was estimated from the LNG spill rate. Some discrepancies can be noticed in the comparison between CFD results and experiments in both the analyzed tests, with the predicted gas cloud footprint being larger than the experimental one.~~ With the same procedure, Wu et al. (2021) ~~benchmarked two well-known CFD codes, i.e., OpenFOAM and Ansys Fluent, for the URANS simulation of the Burro 8 test. The inlet gas velocity was calculated from the LNG spill rate. Predictions indicated an overestimation of the cloud footprints and differences between the two codes. In the works described so far, only the gas phase was considered in the CFD model.~~ Some works suggested applying multi-phase models, which incorporate also the vaporization process of the LNG. For example, Zhang et al. (2015) employed the mixture model with a URANS approach to investigate the LNG vaporization and subsequent gas dispersion, for the Burro 8 and 9 tests ~~and the Coyote 3 and 5 tests. The mass transfer rate between the two phases was determined by a simplified Hertz–Knudsen–Schrage equation, by preliminarily analyzing the sensitivity of results to model constants.~~ Although the more sophisticated modeling approach, results showed that the predicted gas cloud footprint for the Burro 9 test was significantly overestimated compared to the experimental one. A similar approach was employed in (Li et al., 2021) and also there, overestimation of the gas cloud dimension can be noticed.

An important source of uncertainty ~~is then~~ in the numerical simulation of this kind of problems, and, in particular, of the Burro tests, is represented by the value of the LNG pool radius. ~~reached by the~~

~~radius of the LNG pool.~~ It is reasonable to assume that this value can be different from the water pool one; indeed, the experimental images indicate that the LNG covers a limited portion of the water pool. Besides, in the experiments, LNG was spilled over a flat plate; this had the function to spread methane over the water pool, but this fact poses uncertainties on the area occupied by LNG. As a consequence, the real dimension of the LNG pool is unknown and an investigation on this is important to have an accurate numerical setting, to exclude wrong predictions of the quantity of LNG entering the domain, thus leading to wrong gas cloud dimensions.

However, also this last topic is not addressed in the majority of the works in the literature, where authors assume that the radius of the LNG pool is equal to the water pool one~~, i.e. 58 m~~ (Wu et al., 2021; Ikealumba & Wu, 2016; Zhang et al., 2015; Sun et al., 2013). One different treatment is employed in the above mentioned work by (Luketa-Hanlin et al., 2007) who calculated the LNG pool diameter from a mass balance between LNG spill rate and pool evaporation. In such a manner the LNG pool dimension is different from the water pool one.

Finally, another source of uncertainty is the accuracy of CFD models in reproducing the ABL characteristics for different stability conditions, as those encountered in the Burro tests. As a matter of fact, atmospheric turbulence strongly affects the spread of the gas cloud and proper modificatios must be applied to the CFD model to adapt turbulence closure equations to the ABL (Parente et al., 2011; Gorlé et al., 2009; Pontiggia et al., 2009). However, in all the previous works in the literature dealing with numerical simulation of the Burro tests, this issue has not been considered. ~~More specifically, in all the previous works in the literature, stability conditions were taken into account to impose the inlet wind conditions, but no modification of the turbulence closure was incorporated to preserve the profiles along with the computational domain between the wind inlet and the pool region, i.e., to ensure the ABL consistency.~~

From the above literature review a lack of knowledge on the actual influence of inlet conditions in the CFD simulation of gas dispersion from an LNG pool emerges, ~~besides an inaccurate~~ as well as of treatment of LNG pool dimensions and of ABL characteristics.

The present work intends to deeply investigate how the choice of inlet conditions affects the numerical simulation of gas dispersion from an LNG pool ~~corresponding to the LNG pool, affects the numerical predictions of the Burro test series, which is one of the most considered validation cases for numerical models applied in the predictions of hazardous gases release and dispersion, in the framework of process safety studies~~ (Sun et al., 2017). To this purpose, different tests are considered, i.e. the Burro 8 and Burro 9 tests, as they cover the two most concerning classes of atmospheric stability for the dispersion of heavy gases, i.e. slightly stable and neutral, respectively. Contrarily to previous works, the Atmospheric Stability sub-Model (ASsM), proposed by (Pontiggia et al., 2009), is implemented in a single-phase URANS model to accurately reproduce the wind profiles and sustain them in the undisturbed ABL flow before the LNG pool. Furthermore, different values of the turbulent Schmidt number were considered.

For the first time, Uncertainty Quantification (UQ) is applied to gain a deep insight into the boundary

conditions and it is used to calibrate two unknown inlet parameters, i.e. pool radius and mass flow rate, highlighting how the role of these parameters is strongly related to the wind conditions. Moreover, the importance of diffusion and convection in the immission and consequent dynamics of LNG are investigated. Their importance once again depends on the characteristics of the atmospheric boundary layer. ~~Besides, this calibration~~Thus, the present study gives insights on how to set a CFD simulation when dealing with LNG release and subsequent gas dispersion depending on atmospheric conditions and the involved released quantities. In this way, an improved CFD set up is built, thus creating a more accurate tool to perform risk assessment studies and support the development of mitigation measures.

2. Case study

In this work, the Burro series tests (Koopman et al., 1982) have been chosen as a reference since they have been widely studied and used for validation of numerical models in the context of LNG releases and dispersion. This series of tests was performed by researchers of the Lawrence Livermore National Laboratory in 1980 at China Lake and consisted in the release of LNG in the center of a water pool having a diameter of 58 m, with the subsequent monitoring of the gas dispersion through arcs of sensors placed at different distances from the pool, as reported in Fig. 1.

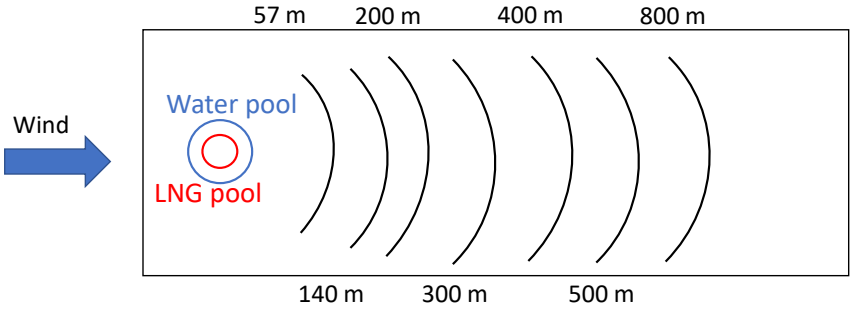

Fig 1: Scheme of the Burro series tests experimental configuration with the indication of the arcs of sensors distances.

Nine different tests were performed, even though a complete set of results is available only for cases 3, 7, 8 and 9. In particular, we considered the Burro 8 and Burro 9 tests as they show interesting features: indeed, the Burro 8 test provides the longest distance reached by the Lower Flammable Limit (LFL) concentration of methane, while the Burro 9 test refers to the highest spill rate. Moreover, these tests are characterized by different atmospheric stability conditions, i.e. slightly stable and neutral for the Burro 8 and 9 test, respectively. Table 1 reports a summary of the experimental conditions for these two tests. Since the effective time variation of the wind speed in the Burro tests is not known, in the following we assume a time-independent velocity profile for the wind, and we consider the mean values reported in Table 1, i.e. 1.8 m/s and 5.7 m/s for Burro 8 and Burro 9, respectively. Indeed, setting the wind speed to the upper boundary of the ranges for the whole duration of the simulations could lead to an over-prediction of the cloud length. The variation of wind speed and direction during the tests could be considered in a future work.

As regards the other two cases, the Burro 3 test was not considered, since it refers to wind conditions similar to the Burro 9 test, while the Burro 7 test was discarded because the LNG cloud is narrow and stretched through sensors.

Table 1: Main experimental conditions for Burro 8 and Buro 9 tests

	Burro 8	Burro 9
Atmospheric stability	Slightly stable	Neutral
Wind speed @ 2 m [m/s]	1.8 ± 0.3	5.7 ± 0.7
LNG spill rate $[m^3/min]$	16.0	18.4
LNG spilled mass [kg]	12070	10285
Duration [s]	100	80

The available experimental data in (Koopman et al., 1982) are the mass flow rate that passes through the arc of sensors placed at 140 m downwind of the pool and the gas cloud footprints and heights. In particular, these last data are available for specific methane concentrations, i.e., 1%, 2.5%, 5% and 10% and times, i.e., $t = 100$ s and $t = 80$ s which correspond to the time in which releases ended for the Burro 8 and Burro 9 test, respectively. In both cases, the total mass that was detected by the sensors and interpolated between the arcs was not equal to the total spilled LNG mass. In particular, a mass of 7439 kg was captured in the Burro 9 test, while 9193 kg in the Burro 8 test, corresponding to 70% and 80%, respectively, of the spilled mass.

Besides, during the Burro 9 test, RPT explosions happened with consequently the first arc of sensors being out of service and a strong variation concerning the mass flow rate data was registered by the sensors placed at a distance of 140 m from the pool. For this reason, the experimental data for Burro 9 have a lower reliability just downwind of the pool. ~~For this reason, some of Burro 9 data were reconstructed through extrapolation, thus implying that lower reliability of the data just downwind of the pool.~~

3. CFD model

The commercial CFD, finite-volume, software Ansys®Fluent 19.2 (Fluent in the following) (Ansys, 2018) was used for the present simulations.

The problem can be described by the unsteady incompressible Navier-Stokes equations, together with the transport equations for the chemical species and the energy equation. These equations were averaged using the Reynolds decomposition, thus leading to the unsteady Reynolds-averaged Navier-Stokes equations (URANS) (1-4):

$$\frac{\partial U_i}{\partial x_i} = 0 \tag{1}$$

$$\frac{\partial U_i}{\partial t} + U_j \frac{\partial U_i}{\partial x_j} = -\frac{1}{\rho}\frac{\partial P}{\partial x_i} + g + \frac{\partial}{\partial x_i}\left[(\nu + \nu_t)\left(\frac{\partial U_i}{\partial x_j} + \frac{\partial U_j}{\partial x_i}\right) + \frac{2}{3}k\delta_{\mathrm{ij}}\right] \tag{2}$$

$$\frac{\partial T}{\partial t} + U_j \frac{\partial T}{\partial x_j} = \frac{1}{\rho c_p}\frac{\partial}{\partial x_j}\left[(k_T + D_t)\frac{\partial T}{\partial x_j}\right] \tag{3}$$

$$\frac{\partial Y_k}{\partial t} + \frac{\partial}{\partial x_i}(U_i Y_k) = \frac{\partial}{\partial x_i}\left[(D_k + D_t)\frac{\partial Y_k}{\partial x_i}\right] \tag{4}$$

where U_i, P, T, Y_k represent the time-averaged velocity in the i-th direction, pressure, temperature and mass fraction of the k-th chemical species (in our case $k = 1, 2$ as we have air and methane). ρ is the density, which is defined as $\rho = \frac{p_{op}}{RT\sum_k \frac{Y_k}{M_{w,k}}}$ with $M_{w.k}$ being the molecular weight of the k-th species, R the universal gas constant and p_{op} the operating pressure, which is the atmospheric one. g is the gravitational acceleration, ν and ν_t are the molecular and turbulent kinematic viscosity, respectively. k represents the turbulent kinetic energy, c_p is the specific heat capacity, k_T the thermal conductivity, D_k the molecular diffusivity of the k-th chemical species. D_t is the turbulent diffusivity and is estimated as:

$$D_t = \frac{\nu_t}{Sc_t} \tag{5}$$

The turbulent Schmidt number Sc_t was set to $Sc_t = 0.4$ as suggested in (Di Sabatino et al., 2007) and (Blocken et al., 2008) for gas dispersion modeling. However, the sensitivity of results to this parameter was assessed by performing simulations also with the standard value, i.e. $Sc_t = 0.7$, as explained in Section 5.

~~A modified version of the standard $k-\epsilon$ turbulence model, proposed by (Pontiggia et al., 2009) to take into account stratification, i.e. the Atmospheric Stability sub-Model (ASsM), was used to determine the turbulent viscosity, i.e. ν_t.~~ A modified version of the standard $k-\epsilon$ turbulence model, namely the Atmospheric Stability sub-Model (ASsM) proposed by (Pontiggia et al., 2009), was used to determine the turbulent viscosity, i.e. ν_t. The ASsM allows to include the Monin-Obukov length within the closure equations of $k-\epsilon$ model in order to obtain consistent profiles of velocity and turbulence for different classes of stability; in particular, the ASsM ~~gives the source term for ϵ reported in Eq. 6 which allows to obtain accurate velocity and turbulence profiles in open-field conditions (empty domain).~~ provides an additional source term $S_\epsilon(z)$ for the turbulent dissipation rate equation, as reported in Eq. 6.

$$S_\epsilon(z) = \frac{u_*^4 \rho}{z^2}\left[\frac{(C_{\epsilon 2} - C_{\epsilon 1})\sqrt{C_\mu}}{\kappa^2}\phi_\epsilon^2\sqrt{\frac{\phi_\epsilon}{\phi_m}} - \frac{1}{\sigma_\epsilon}\left(\frac{2}{\phi_m} - \frac{1}{\phi_m^2} + \frac{T_*}{\kappa T}\right)\right] - \mu\frac{u_*^3}{2\kappa z^3} \tag{6}$$

Moreover, proper wind profiles were set at the inlet of the domain, in terms of velocity (Eq.7), temperature (Eq.8), turbulent kinetic energy (Eq.9) and turbulent dissipation rate (Eq.10) as prescribed in (Pontiggia et al., 2009).

$$u = \frac{u_*}{\kappa}\left[ln\left(\frac{z}{z_0}\right) + \Phi_m(z/L) - 1\right] \tag{7}$$

$$T(z) = T_W + \frac{T_*}{\kappa}\left[ln\left(\frac{z}{z_0}\right) + \Phi_m(z/L) - 1\right] \tag{8}$$

$$k = \frac{u_*^2}{\sqrt{C_\mu}} \tag{9}$$

$$\epsilon(z) = \frac{u_*^3}{\kappa z} \tag{10}$$

In the previous equations κ is the von Kàrmàn constant, i.e. $\kappa = 0.42$, u_* and T_* are the friction velocity and temperature, z_0 the surface roughness, while Φ_m and Φ_ϵ are two functions that depend on z and on the Monin-Obukhov length L. In particular, $\Phi_m = 1 + 5(z/L)$ and $\Phi_\epsilon = 1 + 4(z/L)$. $C_{\epsilon 1}$, $C_{\epsilon 2}$, $C_{\epsilon 3}$, σ_k, σ_ϵ and C_μ are the empirical constants for the $k-\epsilon$ model; their standard values (Jones & Launder, 1972) were adopted here. The possible classes of atmospheric stability are taken into account in the model by properly modifying the Monin-Obukhov length L (Pontiggia et al., 2009), considering $L = \infty$ for the Burro 9 test, which is in neutral stability conditions, and $L = 16.5$ for Burro 8 test, which is in slightly stable conditions.

The 3-dimensional domain was a 950 m × 400 m × 35 m parallelepiped. Dimensions of the domain had been selected to completely describe the spatial development of the cloud during the considered time interval for both cases. The pool was circular and its center, corresponding also to the origin of the reference system, was located at a distance of 150 m from the wind inlet. The computational grid had been made employing the software Ansys®ICEM 19.2 (ICEM in the following) and it consisted of hexahedral cells with a refinement around the pool. The pool had been meshed using an o-grid strategy. ~~In the vertical direction, an exponential refinement towards the ground was imposed.~~ Along the vertical direction, the cell height increased exponentially while moving from the ground. ICEM allows to set the height of the wall-adjacent cell and the total number of nodes, which had been chosen as 36. Moreover, a ratio of 0.13 between the minimum and maximum cell dimensions in this direction had been adopted. Following the recommendations by (Blocken et al., 2007), the height of the wall-adjacent cell centroid z_p

had been set larger than the roughness height, calculated as:

$$K_s = \frac{9.793 z_0}{C_s} \tag{11}$$

where z_0 is the surface roughness, which had been set to $z_0 = 2 \cdot 10^{-4}$ m, corresponding to the terrain roughness as reported in (Koopman et al., 1982). C_s is a constant, which had been set as $C_s = 0.979$ according to the ASsM (Pontiggia et al., 2009).

A preliminary grid independency study had been carried out using different numbers of cells, i.e. 300k, 450k and 900k cells and z_p values, i.e. $z_p = 0.4$ m, $z_p = 0.15$ m, $z_p = 0.05$ m, respectively. The chosen grid had a wall-adjacent cell height equal to 0.3 m ($z_p = 0.15$ m) and a total number of cells ranging from 400k to 460k depending on the pool radius (please see the five cases that have been simulated in next section). According to the reference data (Koopman et al., 1982), the 1% concentration at the second row of sensors (140 m) occurs within an elevation of 7 m, which was discretized with 14 cells in our simulations. In Fig. 2 a scheme of the 3-dimensional domain is reported together with a detail of the mesh in the pool region.

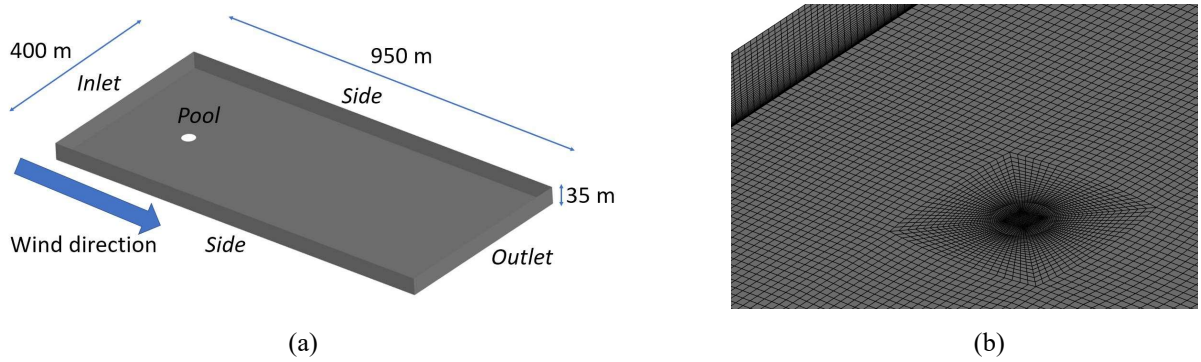

Fig 2: Computational domain (a) and a zoom of the pool region(b).

LNG was treated as pure methane since other heavier hydrocarbons, present in the mixture, have a smaller influence on the duration and dimensions of the flammable cloud (Eberwein et al., 2020). For this reason, the present approach can be considered conservative besides the fact that it allowed to keep a low computational cost for the simulations, since the transport equation was computed only for one species besides air. The pool was modeled as a mass flow inlet with an imposed temperature of 111 K, which corresponds to the LNG vaporization temperature and a methane concentration equal to 1. The present study investigates the impact on the results of the setting of the diffusive and convective terms in Eq.4 at the inlet.

The wind inlet boundary and the top of the domain were treated by imposing the wind speed profiles like in (Marsegan et al., 2016; Pontiggia et al., 2009), while the sides as symmetry boundaries and the outlet as a pressure outlet.

The SIMPLEC scheme was used to handle the pressure-velocity coupling. A first-order implicit method was applied for time advancement with a constant time step of $\Delta t = 0.5$ s corresponding to a

maximum Courant number of ≈ 1; the simulated time intervals for each test case are reported in Table 2. Dedicated tests were performed to check independence of results from the time integration method and the chosen time step. The spatial discretization was performed with a second-order upwind method for all the equations.

4. Methodology for uncertainty quantification and calibration

The methodology used here to calibrate the simulations and hence identify an optimal case setup was based on the generalized Polynomial Chaos (gPC) expansion, which is commonly used in Uncertainty Quantification analysis. This approach consists in building response surfaces for certain quantities of interest (QoI) to some variable input parameters, using a relatively small number of deterministic evaluations.

From a mathematical point of view, gPC is an interpolant method in which a quantity of interest, depending on M random input parameters, represented by a M-dimensional vector $\xi(\omega)$ in the space of events Ω, is projected over an orthogonal polynomial base. This is expressed as follows:

$$QoI(\omega, \boldsymbol{X}) = \sum_{j=0}^{\infty} \beta_j(\boldsymbol{X})\psi_j(\xi(\omega)) \tag{12}$$

where $\psi_j = \phi_j(\xi_1) \cdot \phi_j(\xi_2) \cdot ... \cdot \phi_j(\xi_n)$ is the multivariate j^{th} polynomial of the base, β_j is the j^{th} Galerkin projection coefficient and $\boldsymbol{X}$ represents the field in which the QoI is computed, here the CFD computational domain. The expansion is truncated to a limit T, expressed as:

$$T = \prod_{j=1}^{M}(P_j + 1) - 1 \tag{13}$$

where P_j is the maximum polynomial order for the $j-^{th}$ input parameter.
Then, the orthogonality condition allows to calculate the Galerkin coefficients as follows:

$$\beta_j = \frac{\langle R, \psi_j \rangle}{\langle \psi_j, \psi_j \rangle} \tag{14}$$

in which $< f, g >$ denotes the following scalar product:

$$\langle f, g \rangle = \int w(\xi) f(\xi) g(\xi)\, d\xi \tag{15}$$

with w a weighting function depending on the chosen polynomials. In particular, the integral in Eq. 15 can be computed using the Gauss quadrature rule.

Following this theoretical background, the procedure that was implemented can be summarized as follows:

1. Choose a range of variability for the input parameters.

2. Define a Probability Density Function (PDF) for the variability of the input parameters.
3. Choose the proper polynomial family; the optimal one is orthogonal to a weighting function w equal to the PDF of the input parameters.
4. Define the maximum order of the polynomials, considering a sufficient precision for the interpolation of the QoI.
5. Define the quadrature points for the computation of the integrals in Eq.14. CFD simulations must be carried out for the values of the input parameters corresponding to the quadrature points.
6. Perform the gPC expansion and obtain the response surfaces of the QoI.

The gas release from the LNG pool is affected by many factors, like the amount of spilled LNG, the wind speed and the atmospheric stability conditions. In the Burro tests, the radius of the LNG pool is unknown. As mentioned in the Introduction, some works in the literature assumed this radius to be equal to the one of the water pool, although the LNG pool does not cover the whole water pool. Moreover, the extension of the LNG pool depends on the geometry of the leakage apparatus and the competition between the spill rate and vaporization rate, so ultimately the pool radius is affected also by the wind and atmospheric stability conditions. Since the gas release is modeled with a inlet boundary conditions, the values of the radius and of the mass flow rate dictate the resulting wall-normal velocity of injected methane. This aspect strongly affects the flow field above the pool and the resulting dispersion downwind. In addition, the value of the inlet radius also influences the cross-wind spread of the cloud, particularly in the case of low wind speed. Besides, the vaporization rate is also not known precisely as its measurement is affected by uncertainties as explained in the introduction and underlined in (Luketa-Hanlin et al., 2007). A final remark concerns the choice of the turbulent Schmidt number Sc_t. Despite this parameter affects the overall spatial development of the cloud, it was not included in our stochastic analysis; instead, we selected two different values of Sc_t and assessed its impact on the dispersion. As it will be discussed in the following, the choice of the turbulent Schmidt number is less critical, for the accuracy of the results, than the set up of the inlet boundary conditons.

For these reasons, both pool radius and gas mass flow rate, which depends on the vaporization rate, had been chosen as uncertain CFD input parameters. The gas mass flow rate was chosen to vary in the range from 0 kg/s to the maximum LNG spilled flow rate of each specific case (113 kg/s for the Burro 8 test and 130 kg/s for the Burro 9 test) while the range for the pool radius was taken as $13\,m \div 21\,m$. This last range was determined from an analysis of the case study with the integral dispersion model implemented in DNV GL PHAST 8.1 (PHAST) (DNV GL, 2017), which is widely used for the analysis of accidents involving hazardous materials and risk assessment studies. PHAST solves 1-dimensional equations, together with semi-empirical coefficients to predict phenomena such as pool formation and spreading, and the subsequent gas dispersion. In particular, the lower boundary was selected slightly below the average value evaluated by the integral model, i.e. $R = 13.6$ m. A radius equal to 13 m leads to a vaporization rate of $0.213\,kg/m^2s$ for Burro 8 test and $0.245\,kg/m^2s$ for Burro 9; these values are already higher than those reported in the literature (Luketa-Hanlin et al., 2007) and, then, smaller pool

dimensions were discarded. Moreover, the upper boundary was chosen as the time average between the instant when the radius is maximum, represented in Fig. 3 by the circle, and the one when the release ends, indicated by the square.

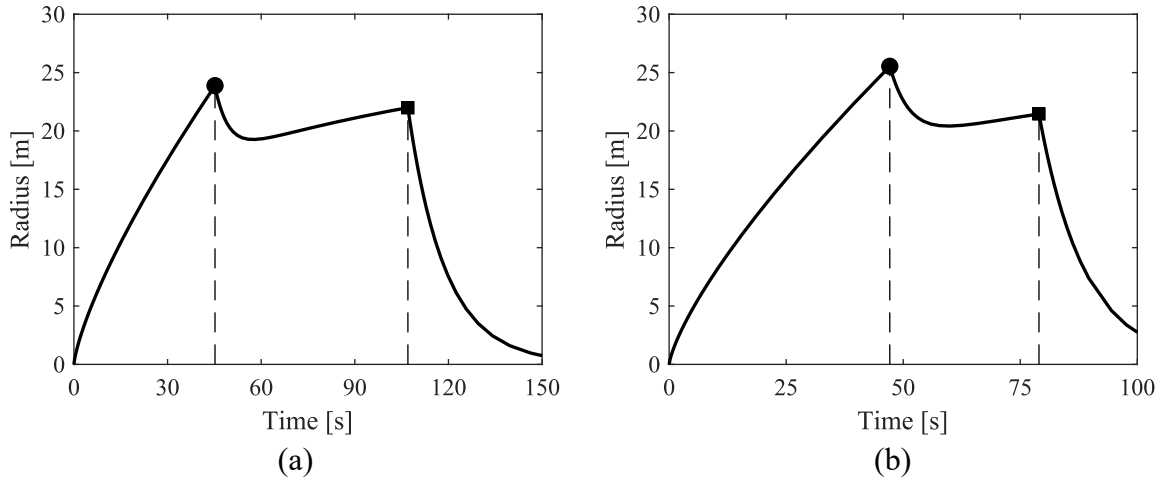

Fig 3: Time evolution of the LNG pool radius in the Burro 8 (a) and Burro 9 (b) tests. The circle represents the maximum radius while the square indicates the end of the release.

A uniform PDF was chosen for both radius and mass flow rate, thus we used Legendre polynomials to perform the gPC expansion as suggested in (Askey & Wilson, 1985). A uniform PDF is often adopted when no specific indication about input parameters variability is available. The maximum order of the polynomials was set equal to 4 and thus, five quadrature points that are collocated as in Fig. 4, were used for each parameter. The calibration of the input parameters was then performed using the computed response surfaces and minimizing the error between the output quantities and the experimental data. In particular, the length of the gas cloud at the LFL concentration, i.e. 5% methane volume fraction, was considered as the target to be fulfilled, to have CFD results matching experimental data. The error between predicted and experimental data was calculated from the following equation:

$$\epsilon_x(R, \dot{m}) = L_{5\%,exp} - L_{5\%,CFD} \tag{16}$$

where $L_{5\%,exp}$ and $L_{5\%,CFD}$ indicate the maximum downwind extension of the five-percent concentration at one meter from the ground ($z = 1$) for numerical and experimental data, respectively. This quantity was chosen instead of the volume of the cloud since, in the experiments, the height development of the methane cloud is reported only for one row of sensors. Nonetheless, the footprint of LFL can already represent a useful quantity for safety. The minimization of the error defined in Eq. 16 ~~this function~~ was carried out with the constraint represented by the amount of methane which is present in the computational domain, that has to be equal to the detected one during experiments. Mathematically, this condition represents a constrained minimization problem with a non-linear constraint, expressed as

follows:

$$\underset{R,\dot{m}}{\text{argmin}}\epsilon_x = f(R,\dot{m}) \tag{17}$$

Since the gPC approximation loses accuracy towards the limits of the variables space, the search of the minimum was performed in a domain bounded by the external quadrature points, i.e. $13.38\,m \div 20.62\,m$ and $\dot{m} = 5.30 \div 107.7\,kg/s$ (Burro 8 test) and $\dot{m} = 6.10 \div 123.9\,kg/s$ (Burro 9 test). The problem was solved in Matlab using built-in minimization functions.

At the end of the procedure, optimal values for the pool radius R and the gas mass flow rate $\dot{m}$ were retrieved.

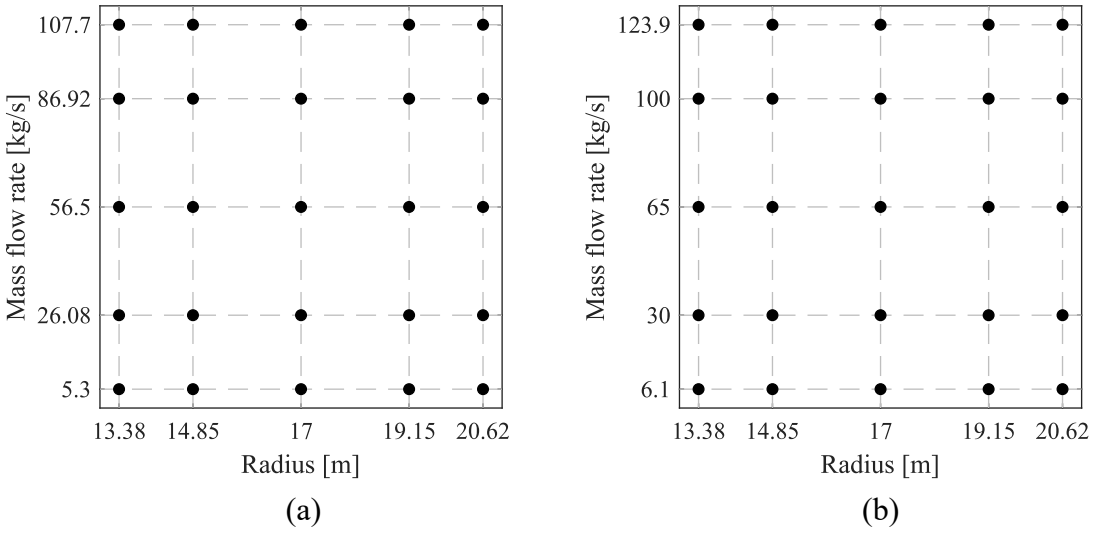

Fig 4: Quadrature points for the radius of the pool and gas mass flow rate for (a) Burro 8 and (b) Burro 9 cases.

5. Results and discussion

Table 2: Summary of RANS simulations setups.

Burro 8			Burro 9					
$U_1(2\,m)$ [m/s]	Time [s]	$\dot{m}$ [kg/s]	$U_1(2\,m)$ [m/s]	Time [s]	$\dot{m}$ [kg/s]	R [m]	Sc_t	Section
		113			130	13.65	0.4	5.1
		0			0	13.65	0.4	5.2
1.8	100	113	5.7	80	130	13.65	0.4	5.3
		[0,113]			[0,130]	[13,21]	0.4	5.4
		[0,113]			[0,130]	[13,21]	0.7	5.4

To better understand the mechanism controlling the amount of gas released from the LNG pool, preliminary simulations were carried out by setting different kinds of inlet conditions. More specifically, we

first considered a convective inlet, at which the entrance of gas by diffusion is not allowed. The results are presented and discussed in Section 5.1. It is worth noting that this is the common approach adopted in the majority of works in the literature (Wu et al., 2021; Sun et al., 2013; Luketa-Hanlin et al., 2007). However, diffusion may also be an important factor determining the entrance of methane in the computational domain. Indeed, the incoming wind dilutes the concentration of methane just above the pool, thus promoting the formation of a concentration gradient in this area that causes diffusion. Hence, a second series of simulations was performed by considering only entrance through diffusion at the inlet and the results are presented in Section 5.2.

All these preliminary simulations were carried out using a gas pool with a radius equal to $R = 13.6$ m, i.e. the average of the radius in time, as predicted by PHAST.

5.1. Purely convective model

As explained in Section 3, the first simulation strategy allows only convection in the transport of methane from the gas pool inlet. This means that the amount of methane that enters the computational domain depends only on the specified gas velocity, which is computed from the imposed mass flow rate and the pool surface area. For the two analyzed cases, the mass flow rate was computed from the spilled LNG, resulting in $\dot{m} = 113$ kg/s for the Burro 8 case and $\dot{m} = 130$ kg/s for the Burro 9 one.

Velocity and methane concentration distributions just above the pool are reported in Fig. 5 to have an indication of the main results in this case. The vertical plane represents the axial velocity, i.e. x-direction (see top panel of the figure) while in the horizontal plane the methane mole fraction is reported to show the gas cloud footprint at 1 m above the ground (see bottom panel of the figure).

In both cases, a recirculation zone is recognizable with negative values of wind speed. This is more pronounced for Burro 9 test where the stagnation zone above the pool causes an increase of velocity in the above region, which reaches a value higher than 9 m/s, that is 30% higher than the maximum value of the wind speed profile. The appearance of a recirculation zone is imputed to the fact that methane has an imposed vertical velocity from the pool, thus creating a cross-flow together with the wind approaching the pool zone.

The main consequence on gas concentration distribution is that mixing above and downwind of the pool is severely increased, thus causing a really large gas cloud which deviates significantly from the experimental observations. Besides, the temporal evolution of the total mass of the released gas appears to be delayed with respect to the data acquired from the monitoring arc of sensors placed 140 m downwind of the pool. A similar behavior was noticed also in (Gavelli et al., 2009) for the Falcon test, in which an increase of the turbulence intensity above the pool reduced this delay in the time evolution. However, there is no physical or practical indication on how to set this quantity, and, thus, it does not seem suitable to use it to improve the accuracy of numerical predictions.

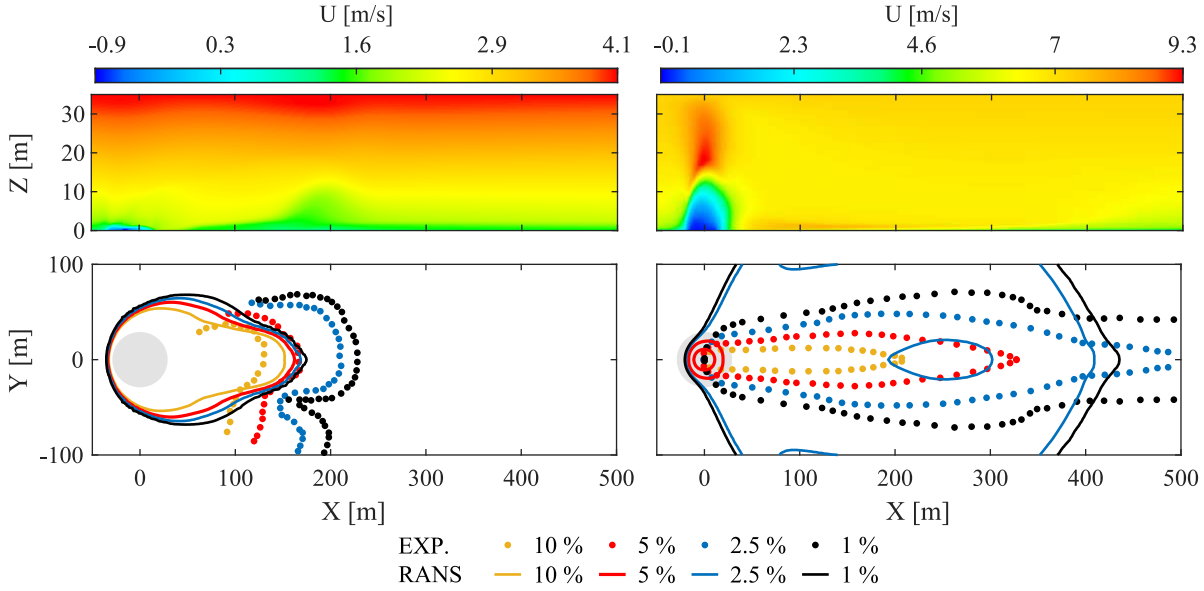

Fig 5: Distributions of the axial component of wind speed on the middle vertical plane and methane concentration footprint at 1 m above the ground for Burro 8 (left column) and Burro 9 (right column) tests with the purely convective model. The gray circle represents the LNG pool, EXP refers to experimental observations of the gas cloud while RANS indicates the CFD results.

5.2. Purely diffusive model

A purely diffusive model was also tested, following the idea in (Pontiggia et al., 2010b). Only the diffusion term in the species transport equation (Eq. 4) for methane at the pool boundary condition was enabled. Using only diffusion for the inlet makes methane mass depending only on the concentration gradient in that particular zone. The resulting flow and concentration fields are reported in Fig. 6.

We notice that the recirculation zone in the velocity field, observed when using a purely convective inlet condition, is not present. This behavior stems from the absence of a vertical velocity component as methane enters the domain without a velocity but just following the Fick law, expressed, for turbulent flows, by the right-hand side of Eq. 4. Anyway, large discrepancies in the gas concentration distribution are still present with an opposite behavior respect to the purely convective model, thus having CFD predictions much smaller than experiments. Moreover, if we impose only diffusion at the pool we lose the control on the methane mass flow rate entering the domain, leading to a serious issue in the reliability of the simulations.

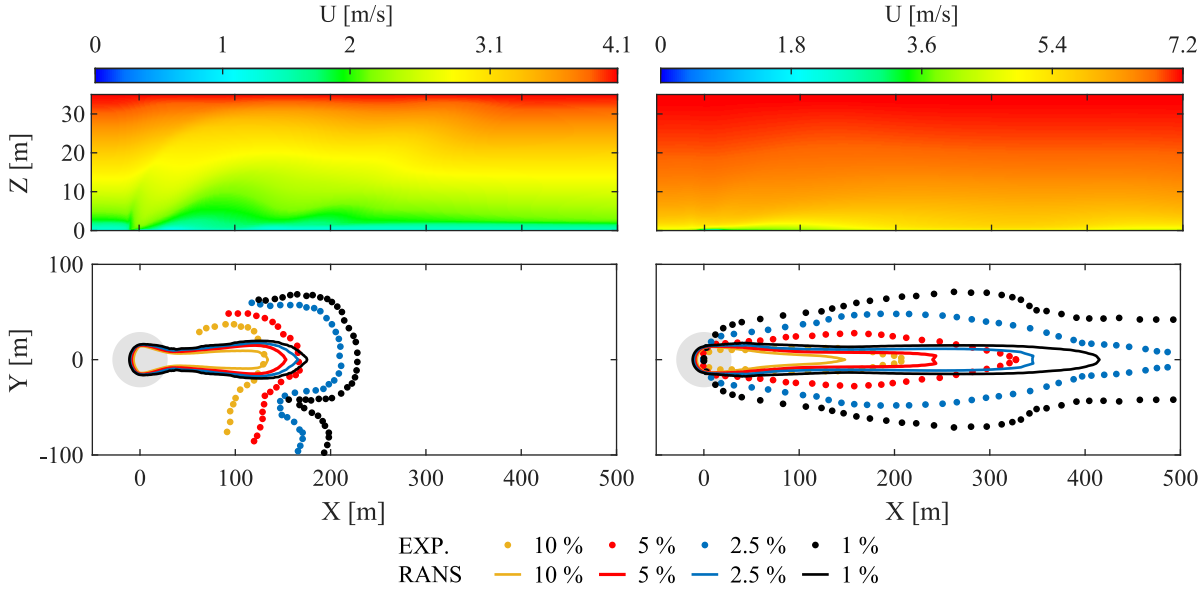

Fig 6: Distributions of the axial component of wind speed on the middle vertical plane and methane concentration footprint at 1 m above the ground for Burro 8 (left column) and Burro 9 (right column) tests with the purely diffusive model.The gray circle represents the LNG pool, EXP refers to experimental observations of the gas cloud while RANS indicates the CFD results.

5.3. Convective-diffusive model

Since both the previous models present errors in the prediction of gas dispersion, a model including convection and diffusion is tested. This way, the treatment of pool boundary condition involves a dependence of the mass on the imposed mass flow rate and concentration gradient as well.

Observing the results obtained with this model, reported in Fig. 7, we can notice that the problems described before are less effective. In fact, recirculation zones in the vertical plane distribution are much smaller with respect to the purely convective model and this leads to plausible gas cloud dimensions, especially when considering LFL concentration.

This preliminary analysis shows that both diffusive and convective phenomena are important for the methane entrance in the computational domain and, therefore, both these terms should be considered when imposing boundary conditions at the pool surface. However, a few issues arise. In particular, the methane mass entering the domain depends on the imposed mass flow rate that is used to calculate gas velocity at the inlet (in the convection term) but also diffusion at inlet takes part in this process. Furtherly, for a given mass flow rate, the inlet velocity strongly depends on the surface area of the LNG pool, and the value $R = 13.6$ m derived from the integral model is affected by uncertainties.

For these reasons, a calibration of these important parameters, i.e., the mass flow rate and the LNG pool radius, is suggested and presented in the next section, considering the convective-diffusive model.

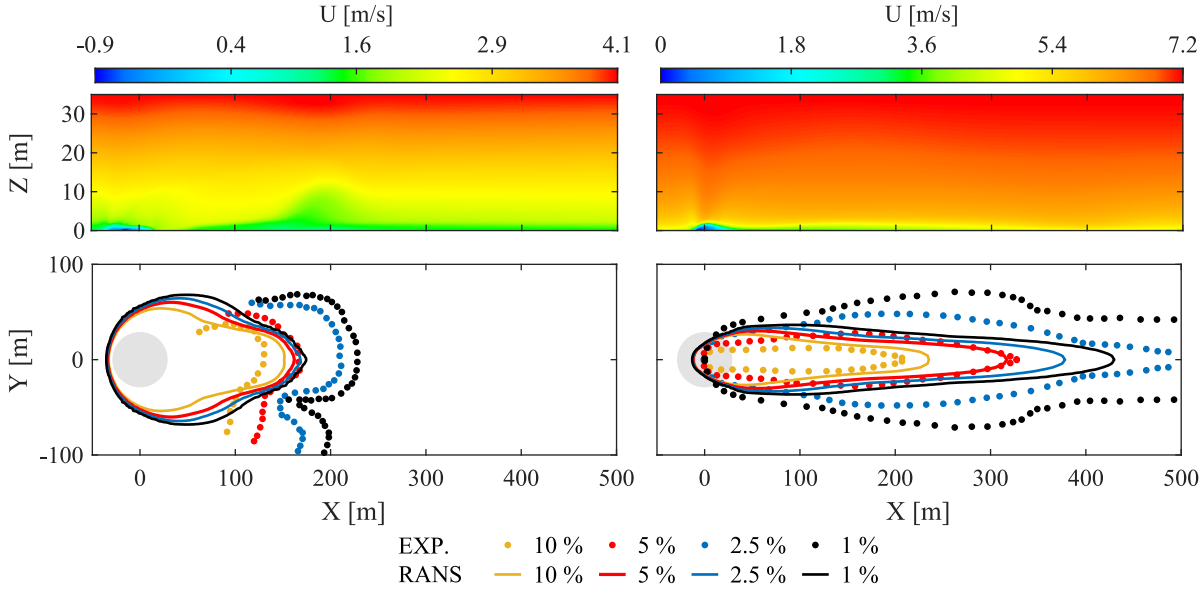

Fig 7: Distributions of the axial component of wind speed on the middle vertical plane and methane concentration footprint at 1 m above the ground for Burro 8 (left column) and Burro 9 (right column) tests with the convective-diffusive model. The gray circle represents the LNG pool, EXP refers to experimental observations of the gas cloud while RANS indicates the CFD results.

5.4. Calibration

The methodology described in Section 4 is employed to perform a calibration of the parameters.

Fig. 8 reports the response surfaces computed with the gPC methodology, of the percentage error in the LFL length and of the methane mass present in the domain for both test cases, i.e. Burro 8 and 9 tests. The red dashed line represents the fulfilment of the mass constraint while the red points indicate the optimal values of the parameters, which minimize the error in the LFL length.

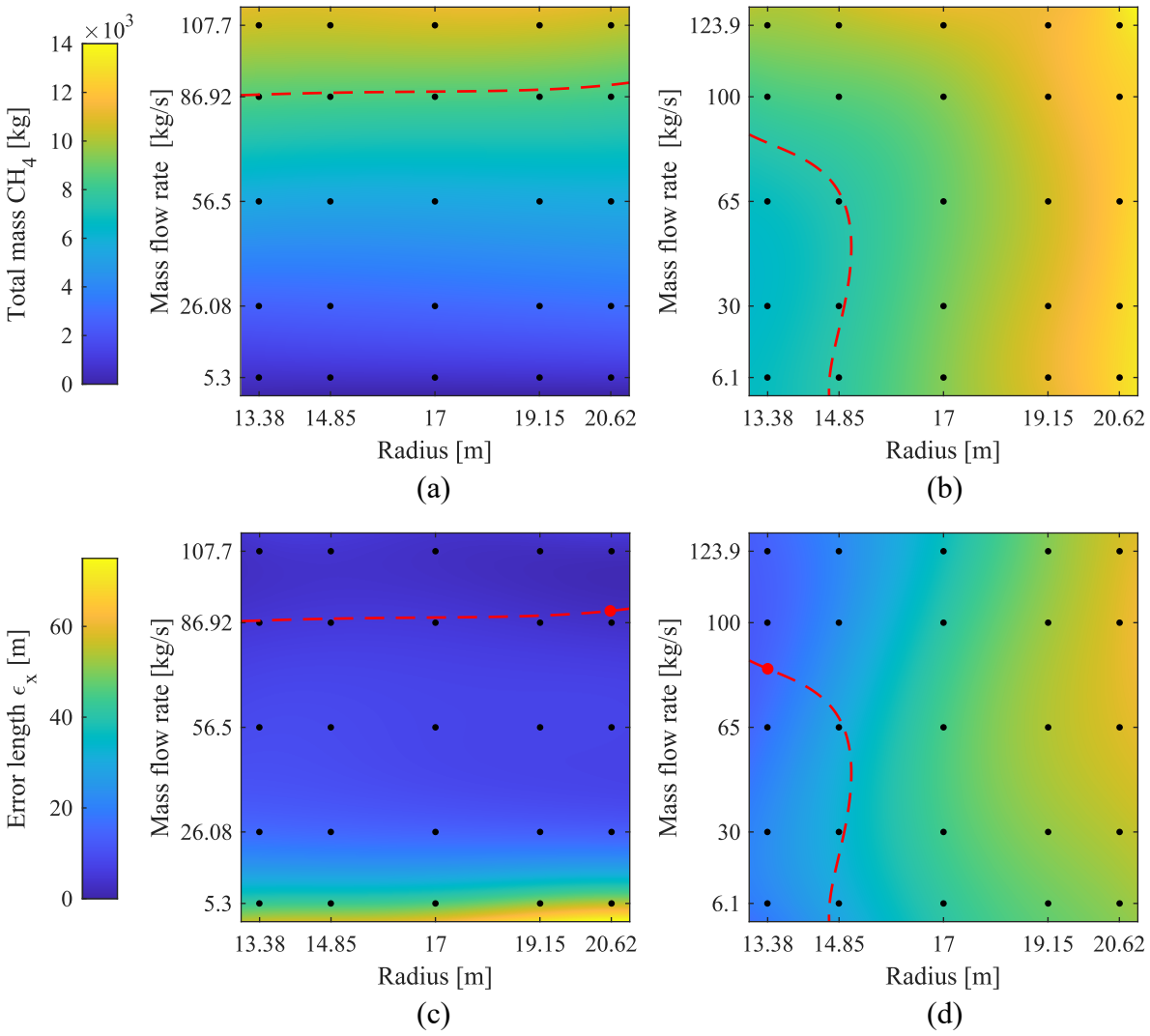

Fig 8: Response surfaces obtained using gPC expansion in the Burro 8 test (a, c) and Burro 9 test (b, d).

The optimal values of the input parameters are chosen ensuring the constraint (dashed line) while seeking for the minimum error. These points are highlighted in the previous figures and correspond to the couple ($R = 20.60$ m, $\dot{m} = 90.35$ kg/s) for Burro 8 test and ($R = 13.38$ m, $\dot{m} = 84.58$ kg/s) for Burro 9.

One important issue that can be highlighted is the small influence of the pool radius on the results for the Burro 8 test; in fact, both the surfaces in Figs. 8 (a) and (c) are almost unaffected by changes in this input parameter. We can explain this behavior by considering that in this case the mass inlet is governed by convection rather than diffusion. Indeed, the low wind speed in the Burro 8 test causes a stagnation of methane just above the pool, hampering the diffusion because of the small methane concentration gradients. For this reason, enabling diffusion has an impact only in the first time-steps of the simulation when methane starts to come out the pool and the gradient is varying.

On the contrary, the behavior of the Burro 9 test shows a remarkable dependency on the pool radius as we can deduce from Figs. 8 (b) and (d). In this case the wind speed is much larger than the one in the

Burro 8 case, resulting in a fast dilution of methane with air leading to a reduced methane concentration above the pool which triggers diffusion.

The comparison between the CFD results using these optimal values and experiments is reported in Fig. 9 for both the gas cloud footprint and the mass detected 140 m downwind of the pool. For the sake of completeness, results obtained in some non-optimal conditions are reported in Appendix A in terms of gas cloud footprints.

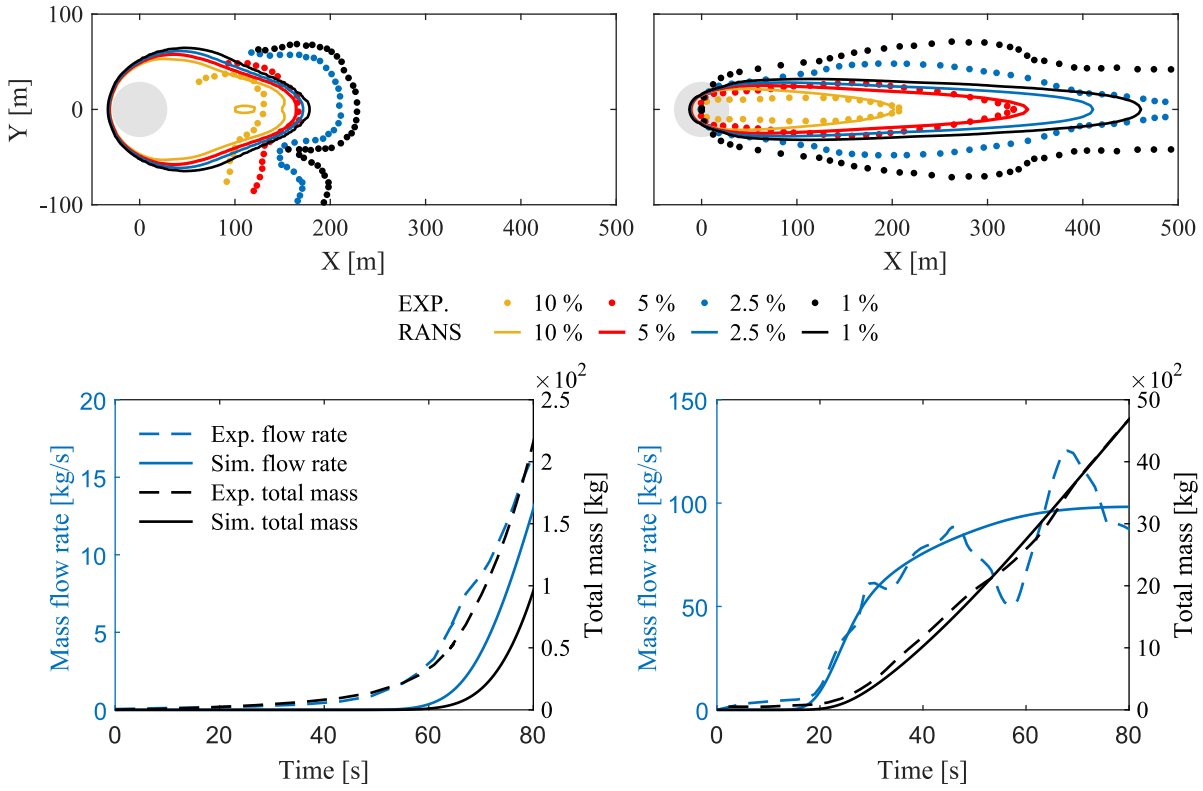

Fig 9: Comparison between experimental data and CFD results using optimal values for Burro 8 (left column) and Burro 9 (right column) tests.

As we can see from the previous figures, the footprint for the 5% concentration is perfectly matched between CFD and experiments in its length and width. Moreover, the temporal trend of both mass flow rate and total mass is also well captured in Burro 9 test and with a sufficient agreement in Burro 8 case. It has to be said that the peaks in the mass flow rate for Burro 9 test are due to the RPT explosions happened during the experiment; hence, these peaks cannot then be predicted by CFD where only the gas phase is simulated.

From the point of view of other volumetric concentrations, there are some discrepancies between CFD and experimental results. This is due to the fact that, at this point, the calibration was performed only for the LFL concentration but a role is also played by the experimental data themselves. In fact, these concentration maps were obtained via an interpolation of the measurements of detectors very far from each other; moreover, the variable atmospheric conditions during the tests could have modified the gas dispersion behavior.

Successively, the optimization problem was solved also for a different value of the turbulent Schmidt number, i.e. $Sc_t = 0.7$, that is the most used value in literature in the simulations of Burro test. This was done to have a deeper understanding on how this parameter can influence the results and to validate the use of the previous value.

Fig. 10 reports the response surfaces obtained in this case, while the results in terms of gas cloud dimensions and mass predicted 140 m downwind of the pool are reported in Fig. 11.

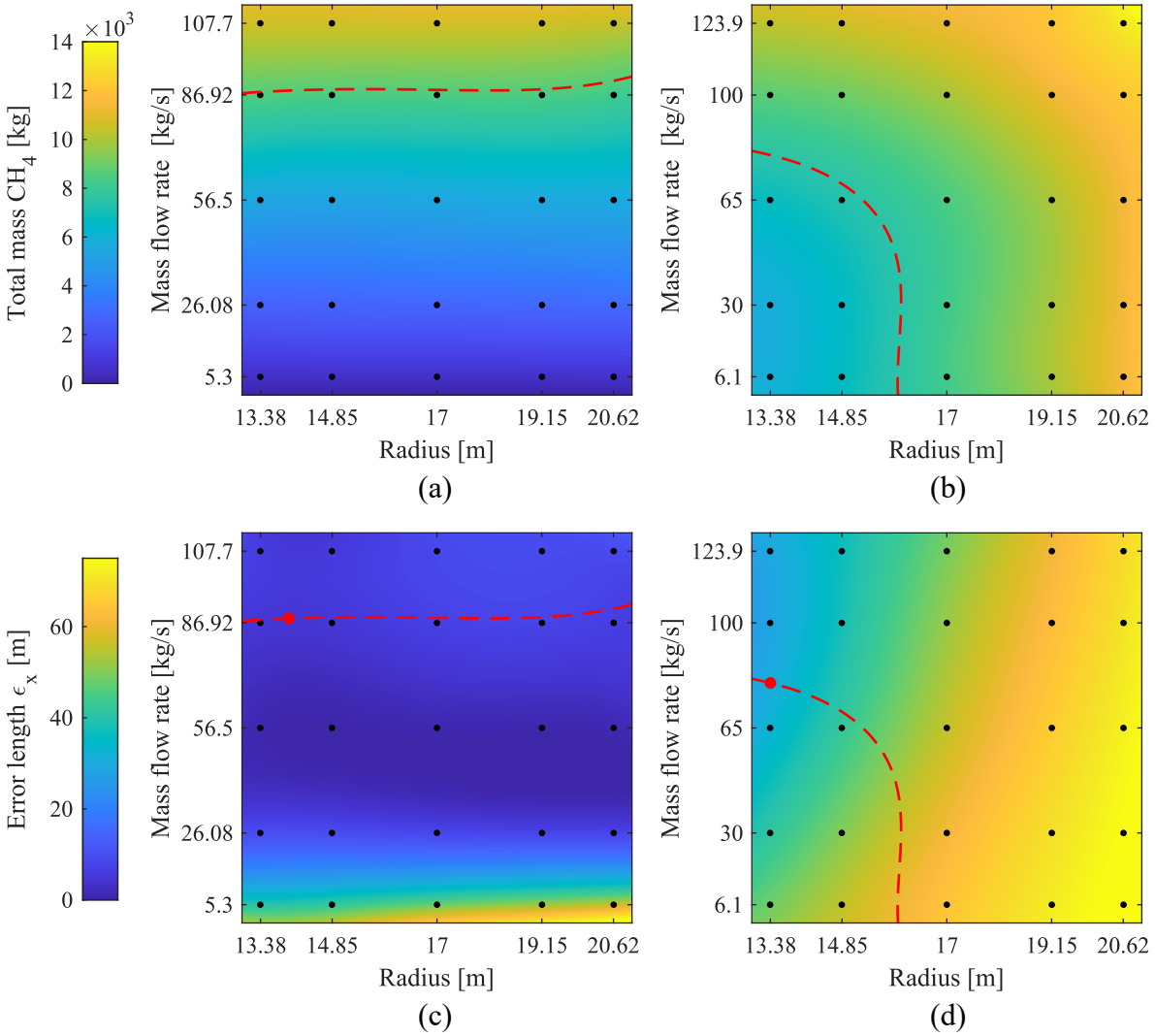

Fig 10: Response surfaces obtained using gPC expansion with the turbulent Schmidt number $Sc_t = 0.7$ in the Burro 8 test (a, c) and Burro 9 test (b, d).

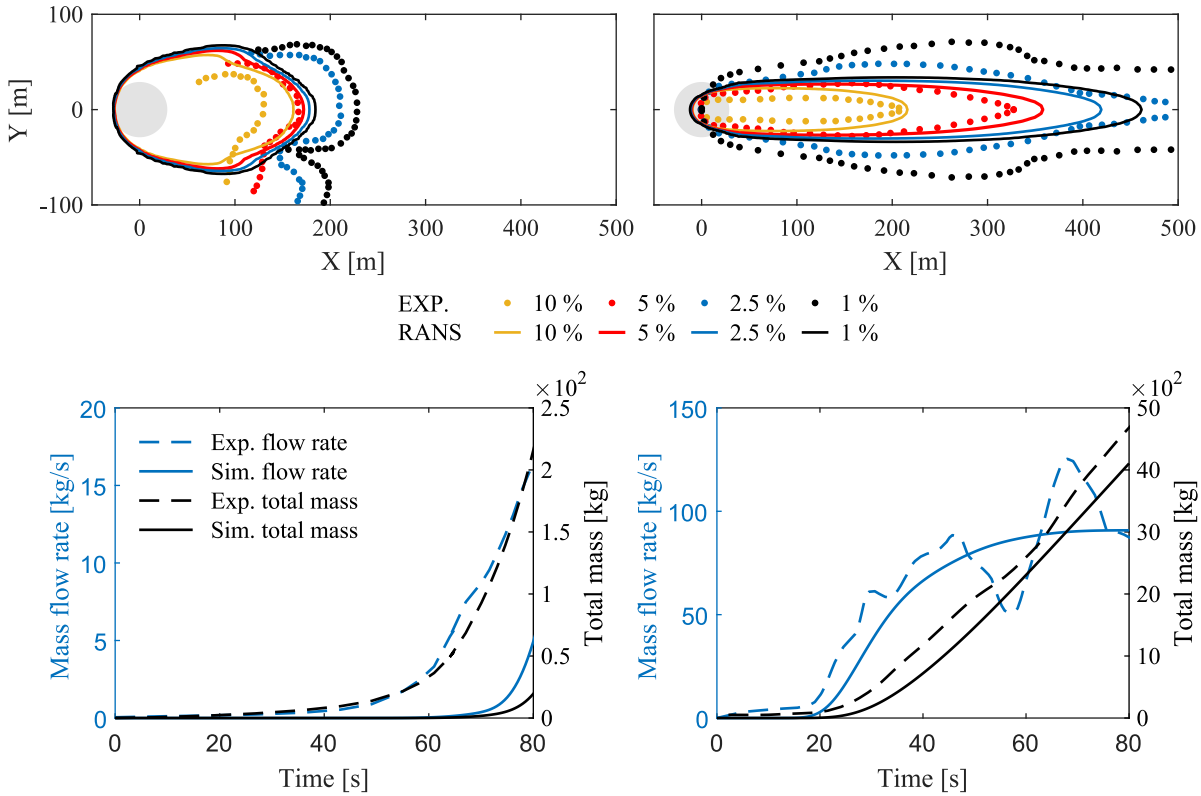

Fig 11: Comparison between experimental data and CFD results using optimal values with $Sc_t = 0.7$ for Burro 8 (left column) and Burro 9 (right column) tests.

Using $Sc_t = 0.7$ for the Burro 8 test, we identified the optimal parameters as $R = 13.96$ m and $\dot{m} = 88.20$ kg/s. Hence we observe a significant reduction of the pool radius (i.e., from $R = 20.60$ m to $R = 13.96$ m when increasing the Schmidt number from $Sc_t = 0.4$ to $Sc_t = 0.7$). However, once again the influence of the pool radius on the numerical predictions is almost negligible. The difference in the optimal flow rate is small (i.e., from $\dot{m} = 90.35$ kg/s to $\dot{m} = 88.20$ kg/s). If we look at the comparison with experimental data, it can be noticed that we have an improvement of the prediction of the gas cloud dimensions, with the value $Sc_t = 0.7$, but the temporal trend of mass presents quite large discrepancies. For Burro 9 test, both gas cloud dimensions and mass temporal trend suffer large differences with experimental data, even when using the optimal values of the parameters identified by the calibration, i.e. $R = 13.38$ m to $\dot{m} = 79.97$ kg/s.

Finally, we can comment that generally the simulations with $Sc_t = 0.7$ show larger deviation from the experimental data than those with $Sc_t = 0.4$. Hence the latter value may be recommended in this kind of studies as also indicated by (Di Sabatino et al., 2007) and (Blocken et al., 2008).

5.5. Discussion

The results showed in the previous sections allow to discuss the advantages of the present methodology on the CFD modeling of gas dispersion in the framework of process safety studies.
Indeed, as mentioned in Section 1, CFD models are reliable tools for risk assessment studies and may

support the development of mitigation strategies. They can serve the consequences assessment of hazardous gas releases and also be used as an important source of data for the implementation of algorithms for the optimal placement of detectors (Cen et al., 2018; Rad et al., 2017). In particular, they can provide accurate predictions of gas dispersion in a high variety of scenarios, even for complex layouts where the well-known integral models fail to cope with the presence of obstacles.

The calibration performed in this study on CFD boundary conditions at the LNG pool has led, for the first time, to a better understanding of the influence of convection and diffusion in the simulations, besides a correct set of boundary values, i.e. gas mass flow rate and the LNG pool radius.

This can have a high impact on the development of CFD models even more accurate in the prediction of the gas cloud dimensions, thus being suitable for risk assessment studies. Besides, the present calibration has shown that wind conditions in terms of velocity and stability are of crucial importance and their modeling within CFD cannot be neglected, giving also to CFD modelers a suitable solution employing UQ analysis.

The present optimization methodology has been applied here to the LFL concentration, but an extension to other levels of gas concentration could possibly help to build an even more accurate and reliable model, with a complete quantification of uncertainties arising from the modeling of pool boundary conditions.

Finally, the present detailed simulation may be adopted to also improve the performance of low fidelity models such as integral ones. Indeed, it can provide computational data useful to derive information about the influence of physical phenomena and different atmospheric conditions on the gas dispersion.

6. Conclusions

The modeling of gas dispersion from an LNG pool, replicating two of the well-known Burro test series, i.e. Burro 8 and Burro 9, has been analyzed in detail to shed light on the treatment of the LNG inlet conditions, in order to build a more accurate CFD model for the analysis of this hazardous gas releases. In particular, a calibration based on a UQ technique is developed, for the first time, to set optimal values of two fundamental parameters, i.e. the pool radius and the inlet gas mass flow rate. Indeed, these values are not known a priori but they are crucial for the gas dispersion behavior. Contrarily to previous works, the influence of convection and diffusion has been analyzed leading to the conclusion that both of them should be considered in the LNG pool inlet conditions. ~~In the tests, LNG is spilled over a water pool; however, it does not cover it entirely. Hence, a first problem is the determination of the real pool radius, which in many works in literature is taken to be equal to the water pool one. A first attempt has been to estimate the pool radius by performing preliminary simulations with an integral model. The time-varying radius has been averaged providing a radius value of 13.6 m (instead of the 29 m of the water pool). Subsequently, different inlet conditions have been set to the inlet boundary. In particular, purely convective and purely diffusive inlet conditions have been observed to lead to unphysical results, with the appearance of extremely large recirculation zones in the first case and a too small amount of inlet mass~~

~~flow rate in the second. The combination of the previous conditions may ensure both the disappearance of the unphysical recirculation regions and the consistency of the total mass flow rate. However, we need to set a specific convective mass flow rate (which is therefore different from the LNG spill rate) in combination with a specific pool radius. To identify the optimal conditions, i.e. mass flow rate and pool radius, a calibration based on uncertainty quantification is applied.~~ Interestingly, the optimal setups were found to be strongly dependent on the wind conditions. For the Burro 8 test, showing the lowest wind speed, diffusion has a significant role and the optimal set indicated a mass flow rate (90 kg/s) which is rather close to the LNG spill rate (113 kg/s) with a slight dependence on the pool radius. ~~In such conditions, diffusion has a significant role only in the first simulation instants, when the concentration gradients above the pool are larger.~~ For the Burro 9 test, the importance of diffusion is lowered by the higher wind speed and the optimal set indicated a mass flow rate of 85 kg/s, much different from the LNG spill rate (130 kg/s). ~~A significant dependency on the pool radius was observed, allowing to estimate a reasonable radius of 13 m. Indeed, in such conditions, the concentration gradients above the pool persist, because of the dilution of the gas above the pool with the inlet air promoted by the high wind speeds.~~ Predictions obtained with the optimal inlet conditions provided results that are in good agreement with experimental data for both the temporal evolution of the methane mass measured downstream of the pool as well as the cloud footprint, reinforcing the reliability of the present calibration methodology. It is worth mentioning that the optimal set was identified by minimizing the errors between experimental and CFD results on the LFL (5%) concentration maps. ~~However, further improvements may be achieved by considering also smaller methane concentrations, as 1% and 2.5%.~~

Besides, two different values for the turbulent Schmidt number have been tested, i.e. $Sc_t = 0.4$ and $Sc_t = 0.7$. Indeed, this parameter is fundamental for gas dispersion and its value has a major impact on the gas cloud dimensions. Results show that the value $Sc_t = 0.4$ gives better agreement with the experimental data with respect to the other one which, however, is the most common used in the literature. ~~The first calibration was carried out for $Sc_t = 0.4$. It was repeated for $Sc_t = 0.7$, which is the most used value in the simulations of Burro tests. Results show that, for the optimal values of the inlet parameters, $Sc_t = 0.4$ gives better agreement with the experimental data. However, a possible improvement of the technique presented here could be to include the turbulent Schmidt number in the list of uncertain input parameters and to perform then a calibration involving a range for this parameter instead of considering just a couple of constant values.~~

Summarizing, the present work has highlighted the need of imposing boundary conditions at the LNG inlet taking into account both diffusion and convection, although their mutual importance is different for different wind speeds and ABL characteristics. ~~Related issues are how to give the inlet convective velocity, i.e., how to set the LNG pool radius if the mass flow rate is given, and the difficulty in controlling the mass because of the diffusion term.~~ Stochastic UQ and parameters calibration show that for low wind speed the crucial parameter is the mass flow rate, which has to be calibrated in order to satisfy the constraint on the methane mass in the domain, while the LNG pool radius has a minor effect on the

result accuracy. Conversely, for larger wind speed, both the mass flow rate and the LNG pool radius have a significant impact. Finally, the same stochastic UQ methodology could be used to quantify the impact of other uncertain parameters, such as the wind speed and direction, on the CFD predictions of this kind of problems. We believe that the present methodology can help to understand the physical processes behind the simulation of gas dispersion from LNG pools and improve the accuracy of CFD models in predicting the dimensions of flammable zones, enabling thus a better design of mitigation measures. Further improvements could be devoted to an optimization based also on lower methane concentration values, such as 1% and 2.5%. Besides, the variability of other parameters influencing the gas dispersion, like wind speed and direction, could be considered in future works, as well as the use of other turbulent Schmidt number values.

Acknowledgments

Support by the University of Pisa through the "Progetti di Ricerca di Ateneo PRA 2020-2021"funding program is gratefully acknowledged.

References

Allegrini, J., Dorer, V., & Carmeliet, J. (2014). Buoyant flows in street canyons: Validation of CFD simulations with wind tunnel measurements. *Building and Environment*, *72*, 63–74. URL: http://dx.doi.org/10.1016/j.buildenv.2013.10.021. doi:10.1016/j.buildenv.2013.10.021.

Aneziris, O., Koromila, I., & Nivolianitou, Z. (2020). A systematic literature review on lng safety at ports. *Safety Science*, *124*, 104595. URL: https://www.sciencedirect.com/science/article/pii/S0925753519322064. doi:https://doi.org/10.1016/j.ssci.2019.104595.

Ansys, I. (2018). *ANSYS® FLUENT® 19.2 Theory Guide*. Cecil Township: ANSYS Inc.

Askey, R. A., & Wilson, J. A. (1985). Some basic hypergeometric orthogonal polynomials that generalize jacobi polynomials. *Memoirs of the American Mathematical Society*, *54*, 0–0.

Bariha, N., Srivastava, V., & Mishra, I. (2016). Theoretical and experimental studies on hazard analysis of lpg/lng release: A review. *Reviews in Chemical Engineering*, *33*. doi:10.1515/revce-2016-0006.

Biltoft, C. (2001). Customer report for mock urban setting test. *Defense Threat Reduction Agency Distribution authorized to U.S. government Alexandria*, (p. 5). URL: http://mech.utah.edu/$\sim$pardyjak/documents/MUSTCustReport.pdf.

Blocken, B., Stathopoulos, T., & Carmeliet, J. (2007). CFD simulation of the atmospheric boundary layer: wall function problems. *Atmospheric Environment*, . doi:10.1016/j.atmosenv.2006.08.019.

Blocken, B., Stathopoulos, T., Saathoff, P., & Wang, X. (2008). Numerical evaluation of pollutant dispersion in the built environment: Comparisons between models and experiments. *Journal of Wind Engineering and Industrial Aerodynamics*, *96*, 1817–1831. doi:10.1016/j.jweia.2008.02.049.

Brown, T. C., Cederwall, R. T., Chan, S. T., Ermak, D. L., Koopman, R. P., Lamson, K. C., McClure, J. W., & Morris, L. K. (1990). Falcon series data report: 1987 lng vapor barrier verification field trials, . URL: https://www.osti.gov/biblio/6633087. doi:10.2172/6633087.

Busini, V., & Rota, R. (2014). Influence of the shape of mitigation barriers on heavy gas dispersion. *Journal of Loss Prevention in the Process Industries*, *29*, 13–21. URL: http://dx.doi.org/10.1016/j.jlp.2014.01.001. doi:10.1016/j.jlp.2014.01.001.

Cant, R., Dawes, W., & Savill, A. (2004). Advanced cfd and modeling of accidental explosions. *Annual Review of Fluid Mechanics*, *36*, 97–119. URL: https://doi.org/10.1146/annurev.fluid.36.050802.121948. doi:10.1146/annurev.fluid.36.050802.121948. arXiv:https://doi.org/10.1146/annurev.fluid.36.050802.121948.

Carboni, M., Pio, G., Mocellin, P., Vianello, C., Maschio, G., & Salzano, E. (2022). On the flash fire of stratified cloud of liquefied natural gas. *Journal of Loss Prevention in the Process Industries*, *75*, 104680. URL: https://www.sciencedirect.com/science/article/pii/S0950423021002862. doi:https://doi.org/10.1016/j.jlp.2021.104680.

Cen, K., Yao, T., Wang, Q., & Xiong, S. (2018). A risk-based methodology for the optimal placement of hazardous gas detectors. *Chinese Journal of Chemical Engineering*, *26*, 1078–1086. URL: https://doi.org/10.1016/j.cjche.2017.10.031. doi:10.1016/j.cjche.2017.10.031.

Conrado, C., & Vesovic, V. (2000). The influence of chemical composition on vaporisation of lng and lpg on unconfined water surfaces. *Chemical Engineering Science*, *55*, 4549–4562. URL: https://www.sciencedirect.com/science/article/pii/S000925090000110X. doi:https://doi.org/10.1016/S0009-2509(00)00110-X.

Di Sabatino, S., Buccolieri, R., Pulvirenti, B., & Britter, R. (2007). Simulations of pollutant dispersion within idealised urban-type geometries with CFD and integral models. *Atmospheric Environment*, *41*, 8316–8329. doi:10.1016/j.atmosenv.2007.06.052.

DNV GL (2017). *Phast & Safeti 8.1 Documentation. Technical Reference - Material Properties.*

Eberwein, R., Rogge, A., Behrendt, F., & Knaust, C. (2020). Dispersion modeling of lng-vapor on land – a cfd-model evaluation study. *Journal of Loss Prevention in the Process Industries*, *65*, 104116. URL: https://www.sciencedirect.com/science/article/pii/S0950423019302256. doi:https://doi.org/10.1016/j.jlp.2020.104116.

Fiates, J., Santos, R. R. C., Neto, F. F., Francesconi, A. Z., Simoes, V., & Vianna, S. S. (2016). An alternative CFD tool for gas dispersion modelling of heavy gas. *Journal of Loss Prevention in the Process Industries*, *44*, 583–593. doi:10.1016/j.jlp.2016.08.002.

Gavelli, F., Chernovsky, M. K., Bullister, E., & Kytomaa, H. K. (2009). Quantification of source-level turbulence during LNG spills onto a water pond. *Journal of Loss Prevention in the Process Industries*, *22*, 809–819. URL: http://dx.doi.org/10.1016/j.jlp.2009.08.015. doi:10.1016/j.jlp.2009.08.015.

Gerbec, M., Pontiggia, M., Antonioni, G., Tugnoli, A., Cozzani, V., Sbaouni, M., & Lelong, R. (2017). Comparison of UDM and CFD simulations of a time varying release of LPG in geometrical complex environment. *Journal of Loss Prevention in the Process Industries*, *45*, 56–68. URL: http://dx.doi.org/10.1016/j.jlp.2016.11.020. doi:10.1016/j.jlp.2016.11.020.

Goldwire, H. C., Jr, Rodean, H. C., Cederwall, R. T., Kansa, E. J., Koopman, R. P., McClure, J. W., McRae, T. G., Morris, L. K., Kamppiner, L., & Kiefer, R. D. (). Coyote series data report. llnl/nwc 1981 lng spill tests dispersion, vapor burn, and rapid-phase-transition. volume 2. appendices, . URL: https://www.osti.gov/biblio/5289356.

Gorlé, C., van Beeck, J., Rambaud, P., & Van Tendeloo, G. (2009). CFD modelling of small particle dispersion: The influence of the turbulence kinetic energy in the atmospheric boundary layer. *Atmospheric Environment*, *43*, 673–681. URL: http://dx.doi.org/10.1016/j.atmosenv.2008.09.060. doi:10.1016/j.atmosenv.2008.09.060.

Guo, D., Zhao, P., Wang, R., Yao, R., & Hu, J. (2020). Numerical simulations of the flow field and pollutant dispersion in an idealized urban area under different atmospheric stability conditions. *Process Safety and Environmental Protection*, *136*, 310–323. URL: https://doi.org/10.1016/j.psep.2020.01.031. doi:10.1016/j.psep.2020.01.031.

Habib, A., Schalau, B., & Schmidt, D. (2014). Comparing tools of varying complexity for calculating the gas dispersion. *Process Safety and Environmental Protection*, *92*, 305–310. URL: http://dx.doi.org/10.1016/j.psep.2014.02.014. doi:10.1016/j.psep.2014.02.014.

Hanna, S. R., Hansen, O. R., Ichard, M., & Strimaitis, D. (2009). CFD model simulation of dispersion from chlorine railcar releases in industrial and urban areas. *Atmospheric Environment*, *43*, 262–270. URL: http://dx.doi.org/10.1016/j.atmosenv.2008.09.081. doi:10.1016/j.atmosenv.2008.09.081.

Horvat, A. (2018). CFD methodology for simulation of LNG spills and rapid phase transition (RPT). *Process Safety and Environmental Protection*, *120*, 358–369. URL: https://doi.org/10.1016/j.psep.2018.09.025. doi:10.1016/j.psep.2018.09.025.

Iannaccone, T., Landucci, G., Scarponi, G. E., Bonvicini, S., & Cozzani, V. (2019). Inherent safety assessment of alternative technologies for lng ships bunkering. *Ocean Engineering*, *185*, 100–114. URL: https://www.sciencedirect.com/science/article/pii/S0029801818320079. doi:https://doi.org/10.1016/j.oceaneng.2019.05.028.

Ikealumba, W. C., & Wu, H. (2016). Modeling of Liquefied Natural Gas Release and Dispersion: Incorporating a Direct Computational Fluid Dynamics Simulation Method for LNG Spill and Pool Formation. *Industrial and Engineering Chemistry Research*, *55*, 1778–1787. doi:10.1021/acs.iecr.5b04490.

Jones, W., & Launder, B. (1972). The prediction of laminarization with a two-equation model of turbulence. *International Journal of Heat and Mass Transfer*, *15*, 301 – 314. URL: http://www.sciencedirect.com/science/article/pii/0017931072900762. doi:https://doi.org/10.1016/0017-9310(72)90076-2.

Jörg Franke, Antti Hellsten, Heinke Schlünzen, B. C. (2007). *Best Practice Guideline for the Cfd Simulation of Flows in the Urban Environment. Cost 732: Quality Assurance and Improvement of Microscale Meteorological Models*. May.

Koopman, R. P., Baker, J., Cederwall, R. T., Goldwire, H. C., Jr, Hogan, W. J., Kamppinen, L. M., Kiefer, R. D., McClure, J. W., McRae, T. G., & Morgan, D. L. (1982). Llnl/nwc 1980 lng spill tests. burro series data report, . URL: https://www.osti.gov/biblio/5679768.

Labovský, J., & Jelemenský, L. (2010). CFD simulations of ammonia dispersion using "dynamic" boundary conditions. *Process Safety and Environmental Protection*, *88*, 243–252. doi:10.1016/j.psep.2010.03.001.

Li, X., Zhou, N., Chen, B., Zhang, Q., Rasouli, V., Liu, X., Huang, W., & Kong, L. (2021). Numerical simulation of leakage and diffusion process of lng storage tanks. *Energies*, *14*. URL: https://www.mdpi.com/1996-1073/14/19/6282. doi:10.3390/en14196282.

Liu, B., Liu, X., Lu, C., Godbole, A., Michal, G., & Tieu, A. K. (2016). Computational fluid dynamics simulation of carbon dioxide dispersion in a complex environment. *Journal of Loss Prevention in the Process Industries*, *40*, 419–432. URL: http://dx.doi.org/10.1016/j.jlp.2016.01.017. doi:10.1016/j.jlp.2016.01.017.

Luketa-Hanlin, A., Koopman, R. P., & Ermak, D. L. (2007). On the application of computational fluid dynamics codes for liquefied natural gas dispersion. *Journal of Hazardous Materials*, *140*, 504–517. doi:10.1016/j.jhazmat.2006.10.023.

Marsegan, C., Busini, V., & Rota, R. (2016). Influence of active mitigation barriers on LNG dispersion. *Journal of Loss Prevention in the Process Industries*, . doi:10.1016/j.jlp.2016.10.010.

Mishra, K. B. (2015). CFD model for large hazardous dense cloud spread predictions, with particular reference to Bhopal disaster. *Atmospheric Environment*, *117*, 74–91. URL: http://dx.doi.org/10.1016/j.atmosenv.2015.06.038. doi:10.1016/j.atmosenv.2015.06.038.

Mishra, S., & Mishra, K. B. (2021). Numerical study of large-scale lng vapour cloud explosion in an unconfined space. *Process Safety and Environmental Protection*, *149*, 967–976. URL: https://www.sciencedirect.com/science/article/pii/S0957582021001555. doi:https://doi.org/10.1016/j.psep.2021.03.034.

Mocellin, P., & Maschio, G. (2016). Numerical modeling of experimental trials involving pressurized release of gaseous co2. *Chemical Engineering Transactions*, *53*, 349–354. URL: https://www.cetjournal.it/index.php/cet/article/view/CET1653059. doi:10.3303/CET1653059.

Moen, A., Mauri, L., & Narasimhamurthy, V. D. (2019). Comparison of k-ϵ models in gaseous release and dispersion simulations using the CFD code FLACS. *Process Safety and Environmental Protection*, *130*, 306–316. URL: https://doi.org/10.1016/j.psep.2019.08.016. doi:10.1016/j.psep.2019.08.016.

Nielsen, M., Ott, S., Jørgensen, H. E., Bengtsson, R., Nyrén, K., Winter, S., Ride, D., & Jones, C. (1997). Field experiments with dispersion of pressure liquefied ammonia. *Journal of Hazardous Materials*, *56*, 59–105. URL: https://www.sciencedirect.com/science/article/pii/S0304389497000290. doi:https://doi.org/10.1016/S0304-3894(97)00029-0.

Osorio-Tejada, J. L., Llera-Sastresa, E., & Scarpellini, S. (2017). Liquefied natural gas: Could it be a reliable option for road freight transport in the eu? *Renewable and Sustainable Energy Reviews*, *71*, 785–795. URL: https://www.sciencedirect.com/science/article/pii/S1364032116311601. doi:https://doi.org/10.1016/j.rser.2016.12.104.

Parente, A., Gorlé, C., van Beeck, J., & Benocci, C. (2011). Improved k-ϵ model and wall function formulation for the RANS simulation of ABL flows. *Journal of Wind Engineering and Industrial Aerodynamics*, . doi:10.1016/j.jweia.2010.12.017.

Pontiggia, M., Derudi, M., Alba, M., Scaioni, M., & Rota, R. (2010a). Hazardous gas releases in urban areas: assessment of consequences through cfd modelling. *Journal of hazardous materials*, *176 1-3*, 589–96.

Pontiggia, M., Derudi, M., Alba, M., Scaioni, M., & Rota, R. (2010b). Hazardous gas releases in urban areas: Assessment of consequences through CFD modelling. *Journal of Hazardous Materials*, *176*, 589–596. doi:10.1016/j.jhazmat.2009.11.070.

Pontiggia, M., Derudi, M., Busini, V., & Rota, R. (2009). Hazardous gas dispersion: A CFD model accounting for atmospheric stability classes. *Journal of Hazardous Materials*, *171*, 739–747. doi:10.1016/j.jhazmat.2009.06.064.

Pontiggia, M., Landucci, G., Busini, V., Derudi, M., Alba, M., Scaioni, M., Bonvicini, S., Cozzani, V., & Rota, R. (2011). CFD model simulation of LPG dispersion in urban areas. *Atmospheric Environment*, *45*, 3913–3923. URL: http://dx.doi.org/10.1016/j.atmosenv.2011.04.071. doi:10.1016/j.atmosenv.2011.04.071.

Rad, A., Rashtchian, D., & Badri, N. (2017). A risk-based methodology for optimum placement of flammable gas detectors within open process plants. *Process Safety and Environmental Protection*, *105*, 175–183. URL: http://dx.doi.org/10.1016/j.psep.2016.10.012. doi:10.1016/j.psep.2016.10.012.

Schleder, A. M., & Martins, M. R. (2016). Experimental data and CFD performance for CO2 cloud dispersion analysis. *Journal of Loss Prevention in the Process Industries*, *43*, 688–699. URL: http://dx.doi.org/10.1016/j.jlp.2016.03.027. doi:10.1016/j.jlp.2016.03.027.

Sun, B., Guo, K., & Pareek, V. K. (2017). Hazardous consequence dynamic simulation of lng spill on water for ship-to-ship bunkering. *Process Safety and Environmental Protection*, *107*, 402–413. URL: https://www.sciencedirect.com/science/article/pii/S0957582017300666. doi:https://doi.org/10.1016/j.psep.2017.02.024.

Sun, B., Utikar, R. P., Pareek, V. K., & Guo, K. (2013). Computational fluid dynamics analysis of liquefied natural gas dispersion for risk assessment strategies. *Journal of Loss Prevention in the Process Industries*, *26*, 117–128. doi:10.1016/j.jlp.2012.10.002.

Tan, W., Wang, K., Li, C., Liu, L., Wang, Y., & Zhu, G. (2018). Experimental and numerical study on the dispersion of heavy gases in urban environments. *Process Safety and Environmental Protection*, *116*, 640–653. URL: https://doi.org/10.1016/j.psep.2018.03.027. doi:10.1016/j.psep.2018.03.027.

Tauseef, S. M., Rashtchian, D., & Abbasi, S. A. (2011). CFD-based simulation of dense gas dispersion in presence of obstacles. *Journal of Loss Prevention in the Process Industries*, *24*, 371–376. URL: http://dx.doi.org/10.1016/j.jlp.2011.01.014. doi:10.1016/j.jlp.2011.01.014.

Tominaga, Y., & Stathopoulos, T. (2007). Turbulent Schmidt numbers for CFD analysis with various types of flowfield. *Atmospheric Environment*, *41*, 8091–8099. doi:10.1016/j.atmosenv.2007.06.054.

Tominaga, Y., & Stathopoulos, T. (2013). CFD simulation of near-field pollutant dispersion in the urban environment: A review of current modeling techniques. *Atmospheric Environment*, *79*, 716–730. doi:10.1016/j.atmosenv.2013.07.028.

Vázquez-Román, R., Díaz-Ovalle, C., Quiroz-Pérez, E., & Mannan, M. S. (2016). A CFD-based approach for gas detectors allocation. *Journal of Loss Prevention in the Process Industries*, . doi:10.1016/j.jlp.2016.03.004.

Wu, J., Cai, J., Yuan, S., Zhang, X., & Reniers, G. (2021). CFD and EnKF coupling estimation of LNG leakage and dispersion. *Safety Science*, *139*, 105263. URL: https://doi.org/10.1016/j.ssci.2021.105263. doi:10.1016/j.ssci.2021.105263.

Zhang, X., Li, J., Zhu, J., & Qiu, L. (2015). Computational fluid dynamics study on liquefied natural gas dispersion with phase change of water. *International Journal of Heat and Mass Transfer*, *91*, 347–354. URL: http://dx.doi.org/10.1016/j.ijheatmasstransfer.2015.07.117. doi:10.1016/j.ijheatmasstransfer.2015.07.117.

Appendix A. Results for non-optimal conditions

To have a complete understanding of the simulations behavior when non-optimal boundary conditions for the LNG pool are used, Fig. A.1 represents the footprints of the concentration maps in some of these cases.

For both the Burro tests considered here, two couples of points in the quadrature points space are chosen. In particular, the couples (R = 18.2 m, $\dot{m}$ = 88.63 kg/s and R = 20.6 m, $\dot{m}$ = 90.39 kg/s) for Burro 8 test and (R = 14.7 m, $\dot{m}$ = 77 kg/s and R = 14.6 m, $\dot{m}$ = 6.19 kg/s) for Burro 9 test, have been considered. All these couples of points respect the constraint of the mass present in the domain but they present higher values of the error on the length of the 5% concentration map with respect to the optimal condition.

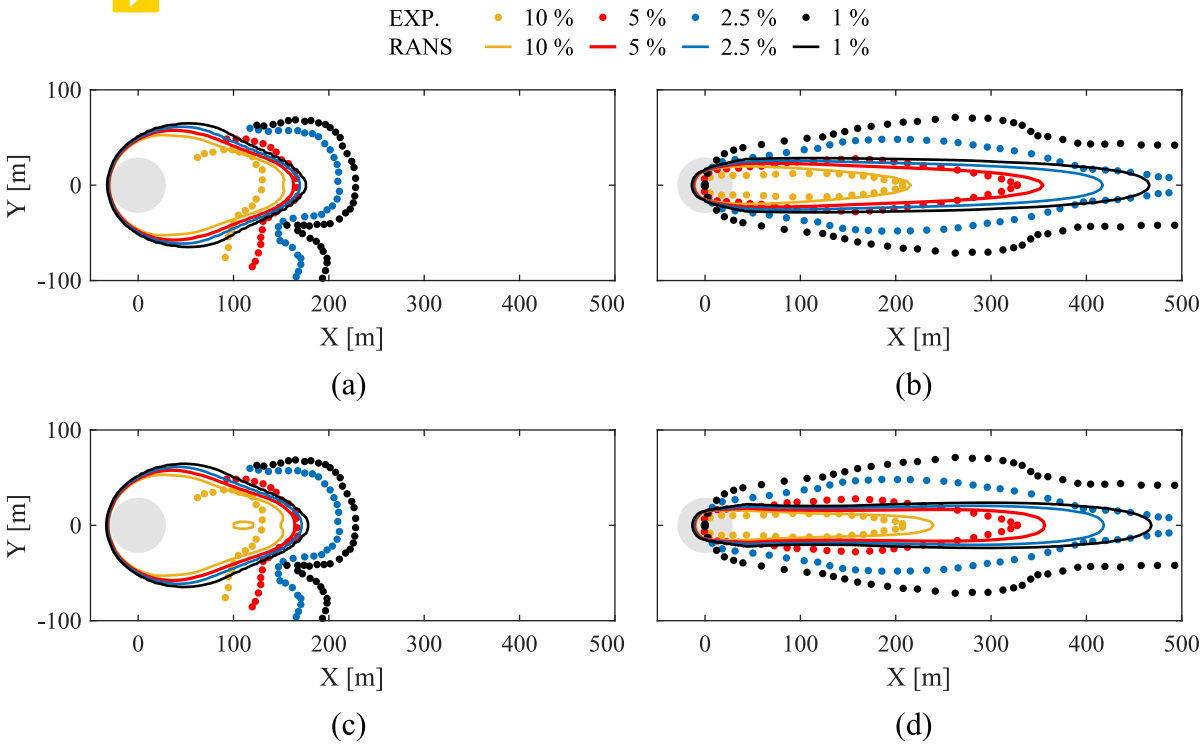

Fig A.1: Comparison between CFD results and experimental data in non-optimal conditions for Burro 8 (left column) and Burro 9 (right column) tests.